J. Fluid Mech. (2005), *vol.* 538, *pp.* 31–69.
doi:10.1017/S0022112005005197 Printed in the United Kingdom

Controlled oscillations of a cylinder: forces and wake modes

By J. CARBERRY[1], J. SHERIDAN[1] AND D. ROCKWELL[2]

[1]Department of Mechanical Engineering, Monash University 3800, Australia

[2]Department of Mechanical Engineering and Mechanics, Lehigh University, Bethlehem, PA 18015, USA

(Received 3 June 2002 and in revised form 24 February 2005)

The wake states from a circular cylinder undergoing controlled sinusoidal oscillation transverse to the free stream are examined. As the frequency of oscillation passes through the natural Kármán frequency there is a transition between two distinctly different wake states: the low- and high-frequency states. The transition corresponds to a change in the structure of the near wake and is also characterized by a jump in the phase and amplitude of both the total and vortex lift. Over the range of flow and oscillation parameters studied the wake states exhibit a number of universal features. The phases of the vortex lift and drag forces have characteristic values for the low- and high-frequency states, which appear to be directly related to the phase of vortex shedding. A split force concept is employed, whereby instantaneous force traces and images allow discrimination between the actual loading and the physics, and their conventional time-averaged representations. The wake states for the forced oscillations show some remarkable similarities to the response branches of elastically mounted cylinders. The equivalence between forced and self-excited oscillations is addressed in detail using concepts of energy transfer.

1. Introduction

Much of the interest in bluff-body flows arises from the practical consequences of having a structure fail as a result of being subjected to fluctuating forces generated by periodic vortex shedding. Usually, these forces have dominant frequencies that, if matched by the structural frequencies of the body, can cause the body to oscillate, usually transversely to the flow. This class of flows has a number of important applications, including vortex-induced vibrations of deep-sea risers, heat exchanger tubes and power lines, as well as structures such as chimneys, bridges and buildings.

Research on bluff-body wakes has had a particular focus on flow over cylinders. The nature of cylinder wakes and the instabilities from which they arise is reasonably well understood, particularly in the light of some of the more recent advances in stability theory, e.g. see Huerre & Monkewitz (1990). These issues become especially important when the response of the wake to self-induced or applied perturbations is being considered. The wake of a stationary cylinder in a free stream is naturally unstable which gives rise to the formation of a Kármán vortex street. Large-amplitude oscillations of the cylinder at frequencies close to the frequency of formation of Kármán vortices can cause significant changes in both the wake structure and the forces on the cylinder. Many studies, including those of Sarpkaya (1978, 1995), Bishop & Hassan (1963), Williamson & Roshko (1988), and Ongoren & Rockwell

(1988) have focused on the response of the wake to forced perturbation and the resulting forces on the cylinder. Bearman (1984) has provided a comprehensive review of the field, which is also extensively discussed in the monographs by Blevins (1990), and Naudascher & Rockwell (1994).

As the frequency of the forced oscillation, f_e, is changed relative to the natural frequency of the stationary cylinder's wake, f_o, there are abrupt changes in both the lift forces on the cylinder and the structure of the near wake. There is a simultaneous jump in the amplitude and phase of the lift force at $f_e/f_o \approx 1$, as first identified by Bishop & Hassan (1963) and subsequently observed by a number of investigators, including Gopalkrishnan (1993), Staubli (1983*a*), Sarpkaya (1978, 1995) and Carberry, Sheridan & Rockwell (2001). Clearly, these changes in the lift force are related to changes in the flow structures in the wake and, while the two effects appear to be mutually reinforcing, the mechanisms which initiate these changes are not well understood.

The changes that occur in the structure of the near wake when f_e approaches f_o have been identified in terms of the mode of vortex shedding in the near wake and the phase (timing) of the initially shed vortices with respect to the displacement of the cylinder. In their extensive mapping of vortex shedding modes, Williamson & Roshko (1988) observed that as f_e/f_o increased though unity there was a change in the mode of vortex shedding from 2P, where two counter-rotating pairs are shed per oscillation cycle, to the 2S or Kármán mode of shedding. Close to $f_e/f_o = 1$ Ongoren & Rockwell (1988) and Gu, Chyu & Rockwell (1994) found, for relatively low amplitudes, a switch in the sign of the initially formed (phase-referenced) vortex in the absence of a change in mode of shedding. Govardhan & Williamson (2000) observed indications of a change in both mode and phase of vortex shedding. In combination, these results suggest that around $f_e/f_o = 1$ there is a change in the structure of the near wake, which corresponds to a jump in the forces on the cylinder.

A switch in the sign of the initially shed vortex as f_e/f_o passes through a threshold value, typically $f_e/f_o \approx 1$, has also been observed for the oscillation of bodies with triangular, square and rectangular cross-sections by Ongoren & Rockwell (1988), Staubli & Rockwell (1989), Lotfy & Rockwell (1993), and Deniz & Staubli (1997, 1998). In their investigation of an oscillating trailing edge Staubli & Rockwell (1989) showed that the switch of the initially shed (phase-referenced) vortex, from one corner of the trailing edge to the other, corresponded to a jump of order π in the phase of the pressure fluctuations on the trailing edge. At the same time there was also a jump in the amplitude of the pressure fluctuations.

Blackburn & Henderson (1999), in their numerical study, established a link between the structure of the near wake and forces on an oscillating cylinder at low Reynolds numbers and a single amplitude A/D of 0.25. They found that the jump in the lift force coincided with a change in the phase of vortex shedding. Carberry *et al.* (2001) found that around $f_e/f_o = 1$ the wake transitioned between two distinctly different states, which exhibited characteristic lift forces and wake structures. At an amplitude ratio of 0.5, the jump in the lift phase and amplitude corresponded to a change in both the timing of vortex shedding and the overall pattern of vortices in the near wake.

The previous literature raises a number of unresolved issues which have motivated the research described in this paper. Despite the fact that the forced oscillation of a cylinder has been the subject of a large number of investigations, the properties of the wake states are still not fully defined. The literature indicates that the jump in the lift forces is a universal feature of these flows, which occurs over a wide range of A/D

and *Re*. However, it is not known how the structure of the wake varies with A/D and *Re*, or if the wake states either side of the transition can be classified in terms of features that occur universally. Many of the questions that we seek to address in this paper concern the transition between different wake states. The ultimate question still remains: what are the mechanisms that cause the wake to transition between the different wake states?

Of significant interest is the question of how forced oscillations relate to the case of a freely vibrating cylinder. The vortex-induced motion of a freely oscillating body is intrinsically coupled with the structure of the wake. By controlling or forcing the motion of the cylinder, the fluid–structure interaction is simplified, allowing the investigation to focus on the response of the wake to a pre-defined motion. The transverse motion of a cylinder undergoing vortex-induced vibrations is generally very sinusoidal and when the cylinder is forced to oscillate, this motion is approximated by a pure sinusoid. However, there are some aspects of these two systems that are fundamentally different: the vortex-induced motion of a body occurs as the structure responds to perturbation from the natural instability of the wake, whereas the forced oscillations perturb the natural instability of the wake causing the wake to respond. The motion of an elastically mounted cylinder relies on positive energy transfer from the fluid to the cylinder. However, as demonstrated by Blackburn & Henderson (1999) and Staubli & Rockwell (1989), when the motion is forced the energy transfer between the cylinder and the fluid may be either positive or negative. Despite these differences, if the sinusoidal forced oscillation accurately represents the vortex-induced motion of the cylinder then the wakes for the two cases should be the same. In this paper, the structure of the near wake and the lift forces for the forced oscillation of a cylinder are compared with the results of Govardhan & Williamson (2000) for an elastically mounted cylinder. Govardhan & Williamson (2000) used two different equations of motion, one involving the total fluid force and the other the vortex force, the latter being associated with a vortex force coefficient and a vortex phase. The phase of the vortex force was linked to changes in the vortex patterns in the near wake, i.e. transformations between the 2P and 2S modes and a switch in the phase of vortex shedding.

The relationship between the wake states of a cylinder that is forced to oscillate and the response branches of a freely oscillating cylinder is particularly relevant to the question of whether the forced oscillations can be used to predict the oscillations of a freely vibrating system. In this paper the similarities and differences between the forced and freely oscillating cases will be considered in terms of the ability of the forced oscillations to predict, or provide insight into, the motion of the freely oscillating case.

2. Experimental method

The experiments were conducted in a free-surface water channel at Lehigh University. The working section was 914 mm wide, 609 mm deep and 5000 mm long, with a turbulence intensity less than 0.1 %. The free-stream velocity, U was varied between $0.056\,\mathrm{m\,s^{-1}}$ and $0.180\,\mathrm{m\,s^{-1}}$, corresponding to *Re* values between 2300 to 9100.

A cylinder was mounted horizontally below the free surface, such that its axis was perpendicular to the free stream. A high-resolution stepper motor was used to oscillate the cylinder transverse to the free stream such that its vertical motion was

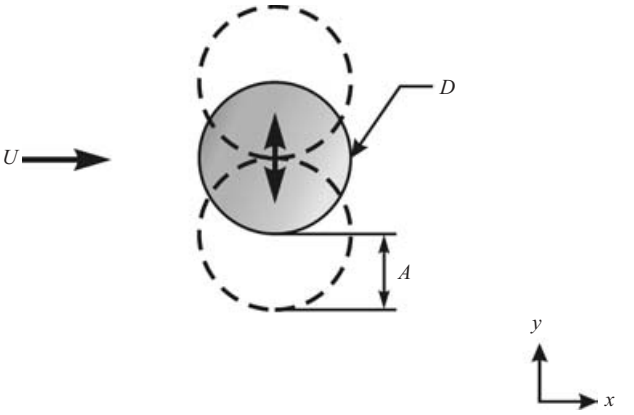

FIGURE 1. Cylinder oscillating transverse to the free stream.

given by

$$y(t) = A\sin(2\pi f_e t) \tag{1}$$

where A is the amplitude of oscillation, generally normalized by the diameter of the cylinder D, and f_e is the frequency of oscillation.

For the range of frequencies studied, the wake was 'locked on' to the cylinder oscillation and the dominant frequency in the lift forces was f_e. In all cases the correlation of the lift signal with a sinusoid was greater than 0.6. Thus, the lift force can be approximated by a sinusoidal function of the form

$$\text{Lift}(t) \approx (1/2\rho U^2 DL)C_L \sin(2\pi f_e t + \phi_{lift}) \tag{2}$$

where C_L is the amplitude of the fluctuating lift coefficient and ϕ_{lift} is the phase with respect to the cylinder's displacement $y(t)$. Both C_L and ϕ_{lift} were calculated in the time domain using data points from over 400 cylinder oscillations.

The orientation and mode of oscillation of the cylinder are shown schematically in figure 1. The experimental set-up was identical to that described in more detail by Carberry *et al.* (2001) and Carberry (2002). Two different cylinders, 25.4 mm and 50.8 mm in diameter, were used, giving aspect ratios of 12.5 and 7.6 respectively. To reduce end effects, the cylinder was fitted with 368 mm diameter end-plates, which oscillated with the cylinder.

The experimental approach was to examine the case of a single amplitude of oscillation ($A/D = 0.5$) at $Re = 2300$ in considerable detail as the frequency of oscillation was varied over the range $0.5 \leqslant f_e/f_o \leqslant 1.4$. This was complemented by a more extensive investigation of parameter space in which the frequency of oscillation was varied for a range of amplitudes ($A/D = 0.25$–0.6) and Reynolds numbers ($Re = 2300$–9100). This approach is reflected in the sequence of results presented later in this paper.

For each value of f_e/f_o, the cylinder started oscillating from rest at $t = 0$, corresponding to the start of the force measurements. Initial transients were recorded in the force data and for most frequencies a steady state was reached after only 3–4 oscillations. Once the cylinder was set oscillating at a prescribed frequency and amplitude, these parameters were fixed. Following each experiment, the cylinder remained stationary in the free stream for a time equivalent to more than 500 Kármán cycles. This procedure is in contrast to a number of other experiments, where the frequency was varied in a continuous fashion while the cylinder continued to oscillate.

The velocity field around the cylinder was measured using the laser-scanning high-image-density particle image velocimetry technique described by Rockwell *et al.* (1993). The flow was seeded with 12 μm silver-coated particles, which were illuminated by a scanning laser sheet produced by passing the beam from a continuous argon-ion laser through a 48 faceted rotating mirror. The images of multiply exposed particles were recorded on 35 mm film and digitised at 106 pixels/mm. The velocity field was calculated by employing a single-frame cross-correlation technique, with an interrogation window of 90×90 pixels and overlap ratio of 0.50. For the 25.4 mm cylinder, the field of view varied between 104.40 mm × 80.31 mm (65×50 vectors) and 171.51 mm × 115.85 mm (74×50 vectors), while the field of view for the 50.8 mm cylinder was 201.45 mm × 158.86 mm (65×51 vectors). The time resolution between successive images was limited by the framing rate of the camera. In general, eight images per cycle were acquired at evenly spaced intervals, starting at the top of the cylinder oscillation. For selected cases, the images were phase-averaged to remove smaller, intermittent structures; they are so designated in the text. To maximize the number of images available for phase averaging, mirror-image fields reflected about the x-axis, i.e. those 180° from the phase point of interest, were included in the phase averaging.

The span-averaged forces on the cylinder in the x- and y-directions were measured using strain gauges configured in two full Wheatstone bridges. For each experiment 5000 data points were sampled at a Nyquist frequency of 6.25 Hz. The inertia forces due to the vertical acceleration of the mass of the cylinder and the supporting sting were calculated and subtracted from the lift force.

3. Comparison with previous work

Over the past three decades, considerable effort has been devoted to characterization of the unsteady lift force acting on a cylinder subjected to forced oscillation. This includes the work of Mercier (1973), Staubli (1983*b*), Gopalkrishnan (1993) and Sarpkaya (1978, 1995). In some cases, these lift characteristics are represented in terms of amplitude and phase, C_L and ϕ_{lift}, or equivalently, in terms of the well-known coefficients C_m and C_d. Figures 2(*a*) and 2(*b*) present the results from a number of previous studies and the current investigation, where the results have been reduced to a consistent format involving ϕ_{lift} versus f_e/f_o and C_L versus f_e/f_o. The open symbols represent data from previous experiments and the filled symbols are from the current investigation. For all cases shown in figure 2 $A/D = 0.5$ while Re varied from 2300 to 60 000. These plots demonstrate generic features that are evident not only in the previous work of Sarpkaya (1978, 1995), Gopalkrishnan (1993) and Staubli (1983*b*), but also in the present study. At low values of f_e/f_o, the amplitude of the lift force is small and out of phase with the cylinder displacement, $y(t)$. For each set of data, as f_e approaches f_o the lift experiences a simultaneous jump in amplitude and phase shift of the order of 180°. Thus, at higher values of f_e/f_o, the lift force has a large amplitude and is approximately in phase with the oscillation of the cylinder.

We describe the sharp changes in the phase and amplitude of the lift force as a transition from a low-frequency lift force to a high-frequency lift force. The frequency at which this occurs is defined as the transition frequency f_t. For the different data sets in figures 2(*a*) and 2(*b*), there is some variation in the transition frequency. Although the reason for this variation is not well understood, Staubli (1983*b*) observed similar variations over a Re range of 25 300–271 000. When the oscillation frequency is normalized by the transition frequency, as shown in figures 2(*c*) and 2(*d*), the

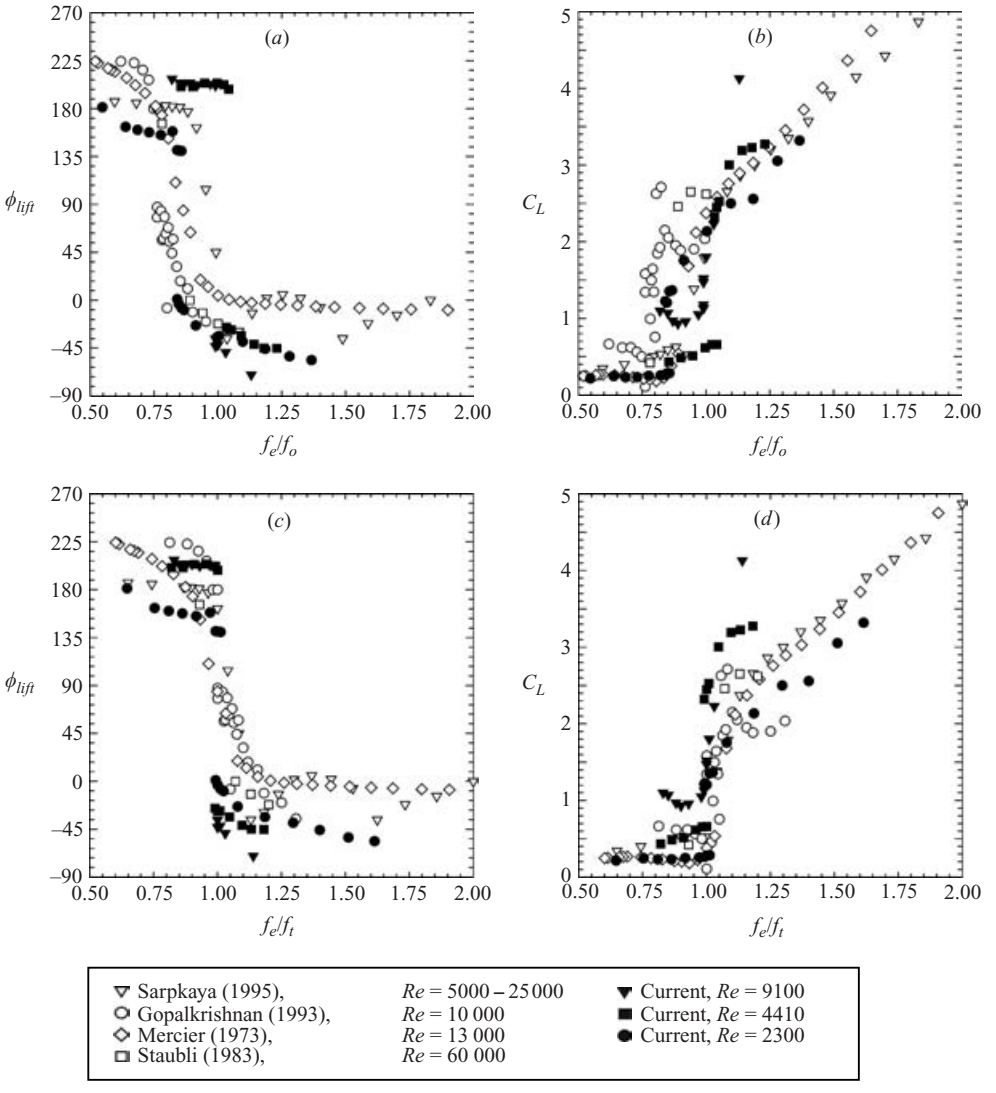

FIGURE 2. Data from previous and present experiment: ϕ_{lift} and C_L as a function of f_e/f_o and f_e/f_t for $A/D = 0.5$.

universal nature of the jump in lift amplitude and phase is clearly evident. Frequency f_o is the natural Kármán frequency of the wake from a stationary cylinder; the frequency of the wake from an oscillating cylinder is expected to deviate slightly from f_o; normalization by f_t accounts for this effect.

Figures 3(a) and 3(b) are a compilation of experimental results in which $C_{D\,mean}$ is plotted as a function of f_e/f_t. The results are for a range of A/D and Re values and include results from the current experiments. In general, $C_{D\,mean}$ has a wide peak around transition but otherwise does not vary strongly with f_e/f_o. Surprisingly, the values of $C_{D\,mean}$ either side of transition are very similar. The general shape of $C_{D\,mean}$ vs. f_e/f_t appears to be independent of both Re and A/D; however as A/D increases $C_{D\,mean}$ is shifted upwards.

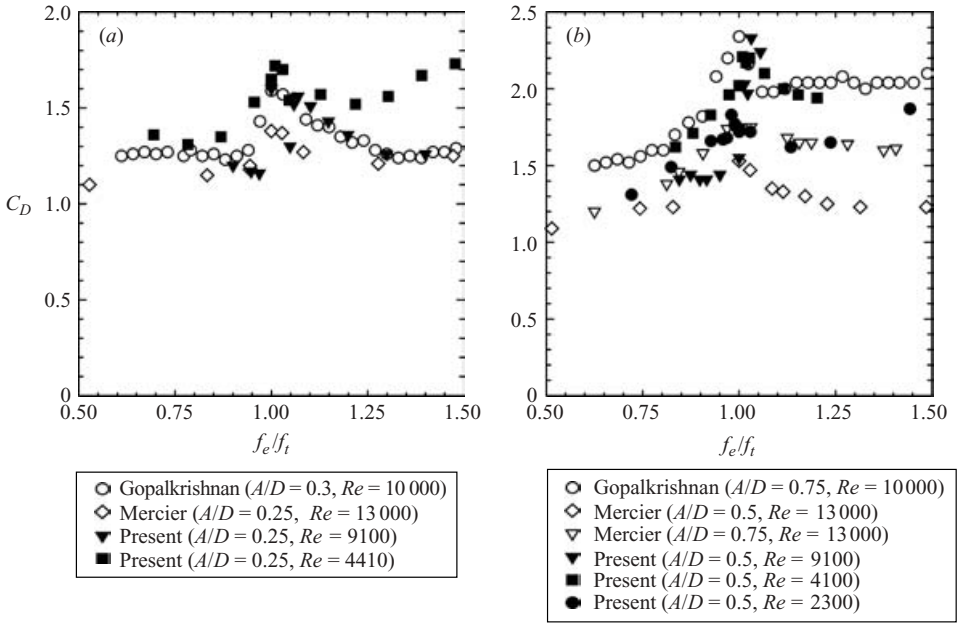

FIGURE 3. Data from previous and present experiments: $C_{D\,mean}$ as a function of f_e/f_t.

4. Wake modes and forces

4.1. *Stable wake states*

Carberry *et al.* (2001) showed that the sharp jump in the phase and amplitude of the lift coefficient corresponds to a change in both the mode and timing of vortex shedding. The instantaneous vorticity fields in figures 4(*a*) and 4(*b*) were both acquired at the maximum (upper) displacement of the cylinder during its motion. Over the range of f_e/f_o studied ($f_e/f_o = 0.5$–2.0), for frequencies of oscillation below the transition, the basic characteristics of the low-frequency wakes were always consistent with the wake shown in figure 4(*a*). Similarly, for f_e/f_o above transition the high-frequency wakes were consistent with the wake shown in figure 4(*b*). In this section, the general features of the two wake states are discussed for a specific set of flow parameters ($A/D = 0.5$ and $Re = 2300$). In fact, the major features of the wake states are very robust, and as will be described below, apply to a wide range of A/D and Re.

The low-frequency wake, shown in figure 4(*a*), generates long attached shear layers which, at higher Re and A/D, often contain small-scale structures. At the top of the cylinder oscillation, the attached negative vorticity extends across the back of the cylinder into the lower half of the wake, while a positive initial vortex forms in the lower shear layer. As the cylinder moves downwards the long negative shear layer splits in two and separate vortex structures are shed into the upper and lower wakes. The negative vortex structures pair up with previously shed positive vortex structures resulting in the 2P mode of shedding, with positive and negative vorticity distributed throughout the vertical extent of the wake. The region immediately adjacent to the base of the cylinder has very low levels of vorticity and velocity. The streamwise extent of this region is a measure of wake length and is analogous to the formation length of a stationary cylinder. As discussed in § 5.1, the size of this region decreases as f_e/f_o increases, although it also depends on A/D and Re.

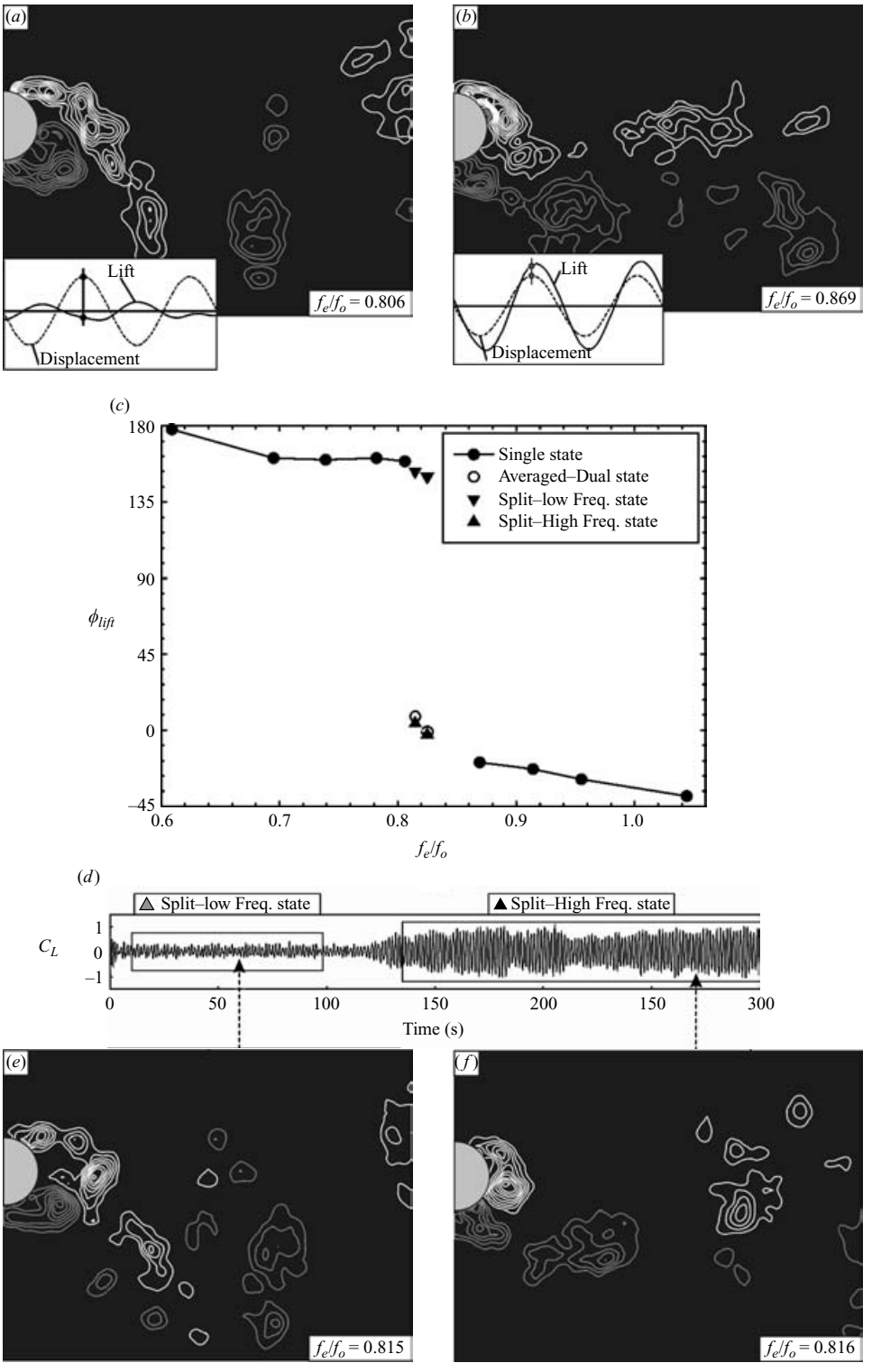

FIGURE 4. For caption see facing page.

In figure 4(*b*), the high-frequency wake vortex structures are shed in the classical Kármán or 2S mode. Negative vorticity is found predominantly in the upper half of the wake, while the lower wake is dominated by positive vorticity. In contrast to the low-frequency mode, the vortex structures form very close to the cylinder and there is virtually no region of low vorticity immediately behind the cylinder. A positive vortex structure is shed into the near wake just after the top of the oscillation and at this point the lower shear layer tends to have a characteristic downwards angle away from the centreline of the wake. The phase of vortex shedding for the high-frequency mode clearly differs from that of the low-frequency mode. For the high-frequency wake in figure 4(*b*), the top of the cylinder oscillation approximately coincides with the shedding of positive vorticity, while at the same phase point in figure 4(*a*) a negative vortex structure is about to be shed from the low-frequency wake. In addition to the difference in the phase of the vortex shedding, figures 4(*a*) and 4(*b*) show a change in the mode of shedding from 2P at low frequencies to 2S at high frequencies. The evolution of these modes was discussed in Carberry *et al.* (2001) and is similar to the modes observed by Govardhan & Williamson (2000), for an elastically mounted cylinder.

In summary, as the frequency of oscillation is varied there exist two distinctly different wake states. For the low-frequency wake state, C_L is small and ϕ_{lift} is large, and the pattern of vortices shed from the cylinder is characterized by the wake shown in figure 4(*a*). For the high-frequency wake state C_L is large, ϕ_{lift} is small and the near-wake structure is as characterized in figure 4(*b*).

4.2. *Transition between wake states*

The jump in the phase and amplitude of the lift coefficient corresponds to a change in both the phase and mode of vortex shedding. These changes represent a transition from one wake state to another. For a small band of frequencies it was found that there could be a transition between the low- and high-frequency wake states while the frequency was held constant. The self-excited transition often occurred after the wake had maintained its first wake state for many oscillations. This concept of self-excited transition was introduced by Carberry *et al.* (2001). In describing the transition between wake states, it is important to specify the manner in which the initial wake state was established. In the present investigation, for each value of f_e/f_o, the cylinder started from rest and the wake state at $t = 0$ was that of a stationary cylinder in a free stream. For $t > 0$ the cylinder was oscillated at a constant frequency until the end of the experiment.

The variation of the phase and amplitude of the lift force through a self-excited transition at $A/D = 0.5$ and $Re = 2300$, is shown in figure 4(*d*). After startup, the wake establishes the low-frequency state within a small number of oscillations: the

FIGURE 4. The instantaneous vorticity fields (*a*) and (*b*) were obtained at the top of the cylinder's oscillation at $f_e/f_o = 0.806$ and 0.869 respectively. The variation of ϕ_{lift} as a function of f_e/f_o is shown in (*c*). The circles, both filled and open, are the average values calculated using the entire lift trace. When the wake undergoes a self-excited transition, the data were split into segments containing either the low- or high-frequency wake state. The values calculated by these segments are represented by the upwards and downwards triangles. An example of the self-excited transition at $f_e/f_o = 0.815$ is shown in (*d*), where the boxes indicate the segments used to calculated the two separate data points. The instantaneous vorticity fields, obtained at the top of the cylinder's oscillation, before ($t = 60$ s) and after the self-excited transition ($t = 270$ s) at $f_e/f_o = 0.815$, are shown in (*e*) and (*f*) respectively.

lift force has a small amplitude and is approximately out of phase with the cylinder's displacement. The low-frequency wake state persists until, at around $t = 97$ s, ϕ_{lift} begins to decrease, followed by an increase in C_L. At $t = 128$ s the wake is in the high-frequency wake state, C_L is relatively large and ϕ_{lift} is close to zero. In between these two states ($97 < t < 128$) there is a region where the lift force is not consistent with either the low- or high-frequency states.

The instantaneous vorticity fields in figures 4(e) and 4(f) were acquired either side of the self-excited transition, at $t = 60$ and 270 s respectively. These images, both at the top of the cylinder's oscillation, clearly depict different wake modes. The wake modes in figure 4(e, f) are consistent with the low- and high-frequency modes in figure 4(a, b) respectively. Thus, when a transition occurs at a single frequency of oscillation the wake states either side of the transition are consistent with the wake states at higher or lower frequencies. For these flow parameters, $Re = 2300$ and $A/D = 0.5$, the self-excited transition always followed the sequence described above; once the high-frequency wake state was established a return to the low-frequency state was never observed.

At any given time the values of C_L and ϕ_{lift} can be used to differentiate between the low- and high-frequency wake states. In figure 4(d), C_L and ϕ_{lift} were used to identify the segments during which the wake was in either the low- or high-frequency state, as indicated by the shaded boxes above the figure. When these segments, each only containing a single wake state, are analysed separately the difference in the forces of the two states is evident. For the lift trace at $f_e/f_o = 0.815$ (figure 4d), three values of ϕ_{lift} are plotted in figure 4(c). The highest value, $\phi_{lift} = 153°$, is calculated from data containing the low-frequency state only ($10 \leqslant t \leqslant 97$). When the lift phase from the high-frequency state ($128 \leqslant t \leqslant 300$) is evaluated, $\phi_{lift} = 4°$. When the wake state is not identified the value calculated is a weighted average of the two wake states.

When time segments that contain only a single wake state are analysed, the forces group into two distinct categories, as can be seen in figure 4(c). The split forces from the low- and high-frequency wake states continue the trend shown by the single-state data at lower frequencies. On the basis of the foregoing, it is evident that the most accurate representation of a data point on a plot of ϕ_{lift} versus f_e/f_o is obtained from consideration of those segments of the corresponding time trace $C_L(t)$ that represent a given wake state, rather than a mixture of low- and high-frequency states.

4.3. *Split forces*

In figure 5, the lift and drag force characteristics as well as the energy transfer are presented as functions of f_e/f_o, for $A/D = 0.5$ and $Re = 2300$. Within the transition region, the time traces have been split into segments containing either the low- or high-frequency wake state. The variation of the force properties over the full range of f_e/f_o is shown in figure 5(a), while in figure 5(b) the transition region has been enlarged to show clearly the variation of selected properties. The split forces from the low-frequency wake state continue the trends shown by the single-state data at lower frequencies. Similarly, the split forces from the high-frequency wake state are consistent with the data at higher oscillation frequencies.

The variation of the phase and amplitude of the lift force in figure 5(a)(i, ii) is consistent with the results of previous experiments shown in figure 2. The 'averaged' values of the lift phase within the transition region are weighted strongly towards the high-frequency state, not only because this state occurred for longer, but also because of the relatively high amplitude and coherence of lift force in the high-frequency wake state. It is possible that results from other studies have been presented with the forces

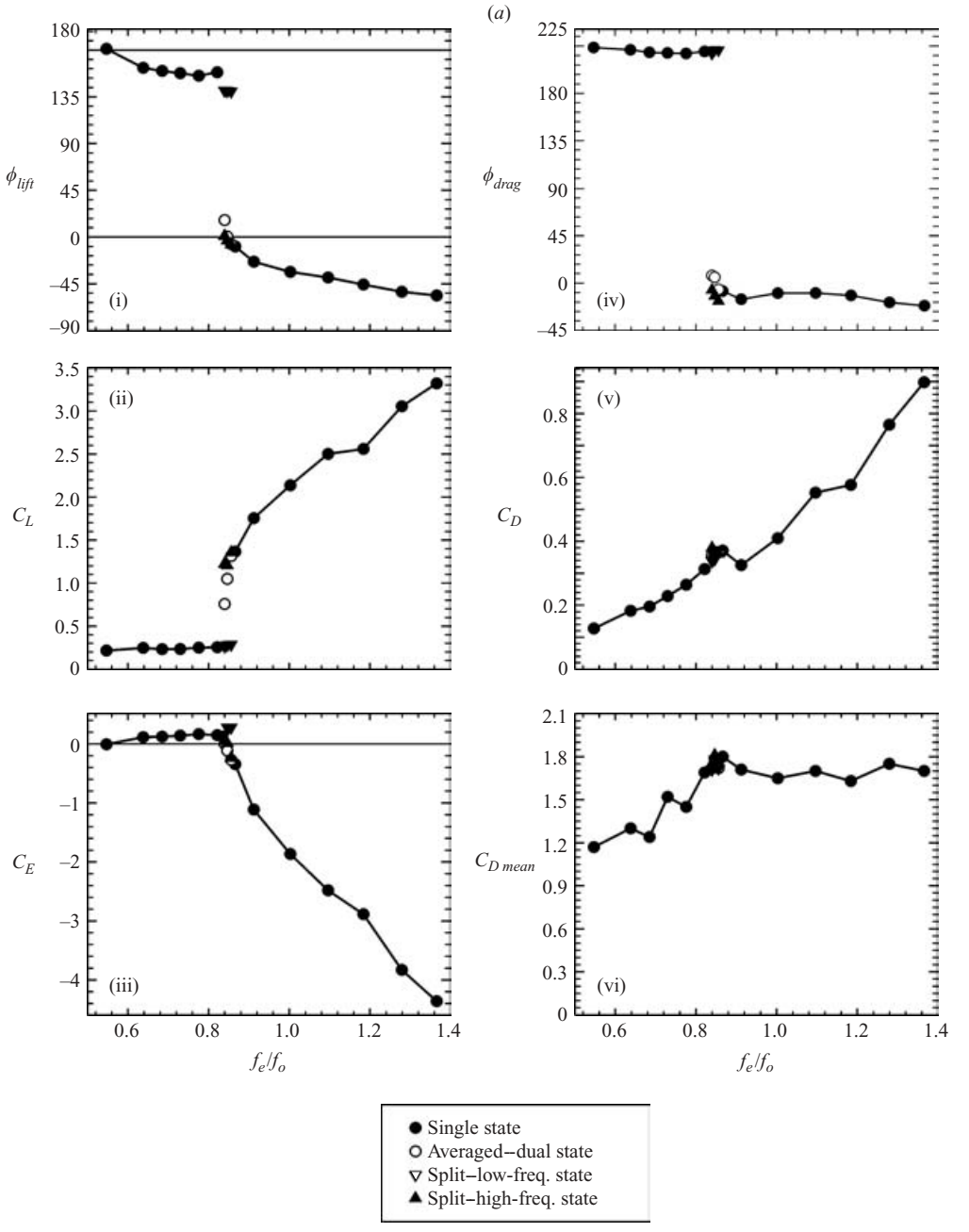

FIGURE 5. For caption see next page.

in this transition region containing a mixture of low- and high-frequency wake states. This observation could explain why intermediate values of ϕ_{lift} have been reported in previous investigations but in our data occur only for points representing more than one wake state. Additionally, as the intermediate values of ϕ_{lift} appear to be linked to the averaging of data from two different wake states this may explain the change in the direction of transition when A/D increased found by Gopalkrishnan (1993).

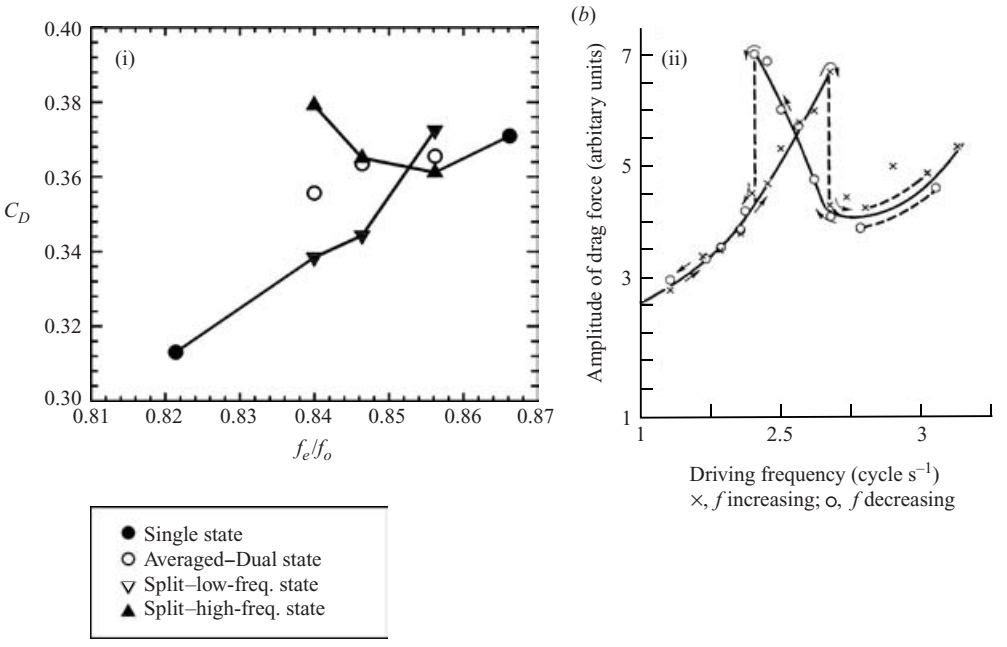

FIGURE 5. (*a*) Variation of the lift, drag and energy transfer with f_e/f_o: (i) ϕ_{lift}, (ii) C_L, (iii) C_E, (iv) ϕ_{drag}, (v) C_D, (vi) $C_{D\,mean}$. The circular data points are the values calculated using the entire data trace: ● representing a single wake state outside the transition region, ○ representing a weighted average of more than one wake state inside transition region. The triangular data points within the transition region represent data segments containing a single wake state only: ▲, low-frequency wake state segment; ▼; high-frequency wake state segment. $A/D = 0.5$, $Re = 2300$. (*b*) (i) Enlarged plots showing the behaviour of C_D in the transition region and for comparison in (ii) the results of Bishop & Hassan (1963) are reproduced showing a hysteretic variation of C_D through transition as f_e/f_o is varied in a continuous fashion.

Energy transfer

The energy transferred between the fluid and the cylinder per cycle is defined as

$$E = \int_0^T \dot{y}\,\mathrm{Lift}(t)\,\mathrm{d}t$$

where

$$\dot{y} = 2\pi f_e A \cos(2\pi f_e t)$$

and the lift is approximated by equation (2): $\mathrm{Lift} \approx (1/2\rho U^2 DL)C_L \sin(2\pi f_e t + \phi_{lift})$. Therefore the normalized energy transfer, C_E, is approximated by

$$C_E \approx \pi \frac{A}{D} C_L \sin(\phi_{lift}). \tag{3}$$

The energy transfer from the fluid to the cylinder is positive when $0° < \phi_{lift} < 180°$; otherwise the energy transfer is negative, i.e. from the cylinder to the fluid. The oscillation of an elastically mounted cylinder requires positive energy transfer. However, a cylinder which is forced to oscillate is not subject to this constraint and all values of ϕ_{lift} are physically possible.

If the lift coefficient is rewritten in terms of its in-phase and out-of-phase components, it can be seen that the energy transfer is proportional to the out-of-phase

component of the lift force:

$$C_L(t) = C_L \sin(2\pi f_e t + \phi_{lift}) = [C_L \cos(\phi_{lift})] \sin(2\pi f_e t) + [C_L \sin(\phi_{lift})] \cos(2\pi f_e t).$$

The variation of the energy transfer between the fluid and the cylinder is shown in figure 5(*a*)(iii). For the low-frequency state, the energy transfer is small, positive and is relatively constant. At transition, there is a sharp increase in C_L but ϕ_{lift} is close to zero, therefore C_E becomes small. As f_e/f_o increases further, C_E becomes increasingly negative.

Drag force

The amplitude of the fluctuating drag force, as well as the magnitude of the time-averaged (mean) drag force, is of obvious physical importance; to date, the phase of the fluctuating drag force has received no attention. The dominant frequency of the drag force is two times the frequency of oscillation ($2f_e$); therefore to relate the phase of the drag to the displacement of the cylinder the general form of the drag force is approximated as

$$\text{Drag}(t) \approx (1/2\rho U^2 DL) C_D \sin[2(2\pi f_e t + \phi_{drag})] + C_{D\,mean} \tag{4}$$

where C_D is the amplitude of the fluctuating drag coefficient, $C_{D\,mean}$ is the mean value of the drag coefficient and ϕ_{drag} is the phase of the drag with respect to the cylinder displacement $y(t)$. Using this definition ϕ_{drag} only has physical significance over a range of 180°, i.e. $\phi_{drag} = \phi_{drag} + 180°$. The drag force tends to be less sinusoidal than the lift force. In all cases, the values of ϕ_{drag} presented were calculated from drag traces whose correlation coefficient with a sinusoidal signal is greater than 0.6. This approach allowed us to calculate values of ϕ_{drag} for all cases except $A/D = 0.25$ at $Re = 4400$. In figure 5(*a*)(iv) ϕ_{drag} is plotted as a function of f_e/f_o. At the transition from the low- to the high-frequency state, figure 5(*a*)(iv) shows that there is a jump in the drag phase of approximately 240° as ϕ_{drag} drops from 225° to −15°. The drag phase is presented such that the jump in ϕ_{drag} at transition is in the same direction and of a similar magnitude to the vortex lift phase, $\phi_{L\,vortex}$, where the behaviour and significance of $\phi_{L\,vortex}$ will be discussed below in § 6.

The overall trend of the drag amplitude, C_D, is to increase with increasing f_e/f_o, with a small peak around transition, as can be seen in figure 5(*a*)(v). This is broadly consistent with the observations of Bishop & Hassan (1963); however, the results obtained by Bishop & Hassan were presented in arbitrary units precluding direct comparison of the two data sets. As shown in figure 5(*b*)(ii) Bishop & Hassan (1963) found a pronounced crossover in the values of C_D over a wide hysteretic transition region by varying f_e/f_o in a continuous fashion. In our case, f_e/f_o was varied in a stepwise fashion with the wake returning to the stationary cylinder state between each value of f_e/f_o. Interestingly, closer examination of the transition region in figure 5(*b*)(i) shows that in our experiments the values of C_D for the low- and high-frequency states 'cross over' between the 2nd and 3rd transition point. The crossover region in figure 5(*b*)(i) is confined to values of f_e/f_o where a self-excited transition occurs; however, the general nature of the crossover is similar to that observed in the hysteretic transition region by Bishop & Hassan.

In figure 5(*a*)(vi), the mean drag $C_{D\,mean}$ shows a small increase as f_e/f_o increases, with a very small peak around transition. These results are consistent with the results of previous experiments shown in figure 3.

While there is an abrupt change in ϕ_{drag} as the wake moves from the low- to high-frequency state, the transition between wake states is not associated with abrupt

changes in C_D and $C_{D\,mean}$. Rather, as either the low- or high-frequency wakes approach the transition there is a relatively small increase in the magnitude of the fluctuating and mean drag forces. Thus, despite the distinct change in the structure of the near wake at transition, the changes in C_D and $C_{D\,mean}$ are relatively small. At other values of A/D and Re, these peaks in C_D and $C_{D\ mean}$ are more exaggerated and in some cases there is a small jump in C_D at transition.

5. Transition between wake states

The transition between the low- and high-frequency states results in significant changes in both the forces on the cylinder and the structure of the near wake. Therefore it is clearly important to have an understanding of why and how this transition occurs. A transition between two states occurs in a large number of flows, for example the transition between a laminar flow and a turbulent flow. However, determining the exact origin of a transition between two different states is a very difficult problem. Using stability theory, it is often possible to determine how the stability of a system changes leading up to and during a transition, but such analyses do not necessarily explain why the system is changing. Generally speaking, transitions occur when the controlling parameter, in our case f_e/f_o, reaches a critical value. Further changes in the controlling parameter cause the original state to become unstable and the system moves to a new state. The variation of the forces on the cylinder as f_e/f_o approaches transition, in particular the almost constant values of ϕ_{lift} and ϕ_{drag} shown in figure 5(a)(i, iv), give very little indication that transition is about to occur. In this section we examine the systematic changes in the structure of the near wake as f_e/f_o increases toward transition, as well as the changes in the nature of the self-excited transition as f_e/f_o increases within the transition region.

5.1. *Wake length*

The vorticity fields in figure 6 show the changes in the structure of the near wake as f_e/f_o increases from 0.695 to 0.869. The vorticity fields were calculated by phase averaging nine consecutive images at the extreme displacement of the cylinder, with the exception of the image at $f_e/f_o = 0.782$, where only seven images were available. These images represent a 'short term' average of the wake structure and demonstrate the subtle changes of the two wake modes with frequency. The decrease in the peak vorticity due to the averaging of instantaneous vorticity fields did not vary with either f_e/f_o or wake state, indicating that the level of fluctuation in the vorticity fields is approximately constant.

Figure 6(a) shows the low-frequency wakes as f_e/f_o increases from 0.695 to 0.815. As f_e/f_o increases the general mode of shedding is unchanged but there is a decrease in the streamwise length of the attached vortex structures. Over this range of frequencies, ϕ_{lift} and ϕ_{drag} are approximately constant. Additionally, in § 6.3 $\phi_{L\,vortex}$ will also be shown to be essentially constant. Therefore, the changes in the position of the vortex structures in figure 6(a) are not phase related but are due to a contraction of the wake. These observations are consistent with those of Ongoren & Rockwell (1988), and Gu *et al.* (1994).

At $f_e/f_o = 0.8154$ and 0.825 a self-excited transition from the low- to the high-frequency state was observed. For $f_e/f_o = 0.815$ the low- and high-frequency modes are shown in figure 6(a)(v) and figure 6(b)(iii) respectively, where for the high-frequency mode the vorticity is wrapped tightly around the cylinder and the wake length is clearly shorter. The vorticity fields in figure 6(b)(i, ii) at $f_e/f_o = 0.825$ were

acquired at two separate time periods when the wake appeared to be between the low- and high-frequency wake states and the values of C_L and ϕ_{lift} were not fully consistent with either the low- or high-frequency state. The corresponding structure of the near wake is not fully consistent with the low-frequency wakes in figure 6(*a*) or the high-frequency wakes shown in figure 6(*b*)(iii, iv) and can be described as an intermediate wake state.

Although visual inspection of figure 6 reveals a contraction of the wake as f_e/f_o increases, there is no single, universally accepted method to calculate the length of the wake. Historically, the wake formation length of a stationary cylinder has been defined in a number of ways, generally using a series of point measurements with high temporal resolution. Our PIV data have limited temporal resolution but high spatial resolution and we choose a different method to represent the wake length using a fixed phase point. The variation of the wake length at the top of the cylinder's oscillation can be quantified by calculating L_{cpv}, the streamwise distance from the base of the cylinder to the centroid of the attached positive vorticity. The region of attached vorticity was defined by applying a threshold minimum vorticity level to determine the boundary. Due to the experimental difficulties in resolving the boundary layer around the front of the cylinder, L_{cpv} was calculated by taking moments of the attached positive vorticity downstream of the centre of the cylinder. A schematic demonstrating the definition of L_{cpv} is shown in figure 6(*c*). L_{cpv} is not a direct measure of wake length, but is a property which appears to vary directly with the wake length and is also easily quantified at a particular phase point. Moreover, for the case of an oscillating cylinder the phase-referenced length of the attached positive vorticity appears to be related to the transition between the low- and high-frequency wake states. Figure 6(*c*) shows that as f_e/f_o increases from 0.695 towards transition the wake remains in the low-frequency state but L_{cpv} decreases. However, as f_e/f_o increases further, the low-frequency state is no longer stable and there is a transition from the low- to the high-frequency state. The variation of L_{cpv} with f_e/f_o shows that the transition to the high-frequency wake corresponds to a contraction of the wake below a certain critical length. For frequencies within the transition region, after startup the wake moves to the low-frequency wake state and the wake length is very close to the critical value. There is some variation in the wake length from cycle to cycle; however, after the transition to the high-frequency state the wake length is significantly shorter. Interestingly, at transition L_{cpv} becomes negative, i.e. the centre of the positive vorticity moves back behind the rear of the cylinder. However, the fact that there is of change in sign of L_{cpv} at transition is not necessarily physically significant, as the calculation of L_{cpv} does not include all attached positive vorticity and is calculated at a particular phase point in the cylinder's oscillation.

In the light of the changes in the length of the near wake preceding the transition to the high-frequency state, observed in both this and previous work, it is reasonable to suggest that the wake length plays a role in the transition. The most robust feature of the transition is the large shift in the phase of vortex shedding. Vortex shedding depends on the interaction between the two shear layers, and as the wake contracts, this interaction is altered. The contraction of the wake as f_e/f_o increases towards transition does not result in significant changes in the mode or phase of vortex shedding. However, the contraction of the wake below a critical length coincides with the transition and a change in the way the shear layers interact. If the interaction, which originally resulted in vortex shedding at a particular phase point, is significantly altered by the contraction of the wake below a critical length, then it may have been the cause of the transition to the different stable wake state. For the case of the

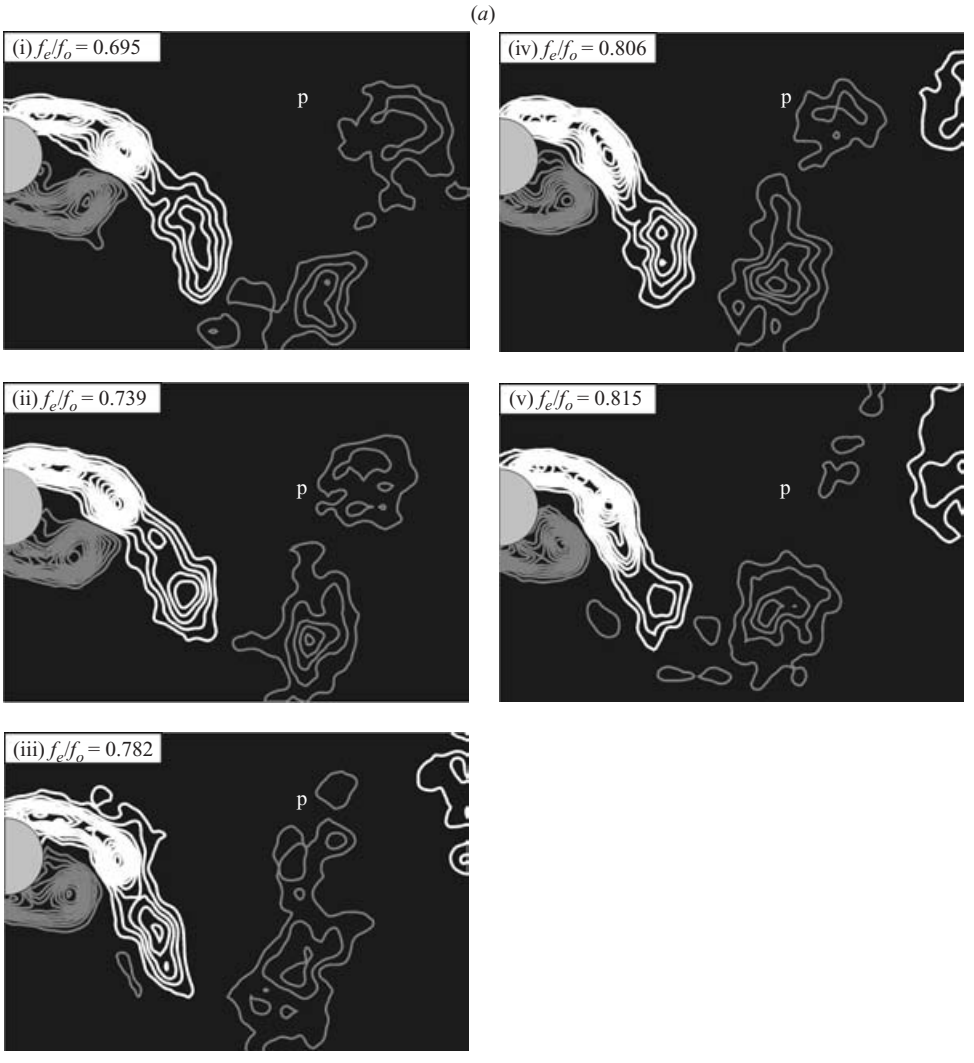

FIGURE 6(*a*). For caption see facing page.

oscillating cylinder, after the transition to the new wake state, the vortex shedding occurs at a very different phase point and at $A/D = 0.5$ there is a change in the mode of vortex shedding from 2P to 2S.

As f_e/f_o increases towards transition there is an increased disparity in the relative strength of the vortices in the '2P pairing'. This is demonstrated in figure 6(*a*), where as f_e/f_o increases, there is a decrease in the strength of the positive vortex structure, designated by the letter P, which has been shed into the upper wake. Although this field of view does not show the pairing of the positive and negative vorticity, the symmetry of vortex shedding means that the relative strength of the upper and lower positive vortex structures is indicative of the relative strength of the vortices within the counter-rotating pairs, i.e. the weaker positive vortex in the upper wake forms a counter-rotating pair with a stronger negative vortex. The formation of the 2P mode depends on the shear layers shedding two separate structures. In figure 6(*a*)(i–v),

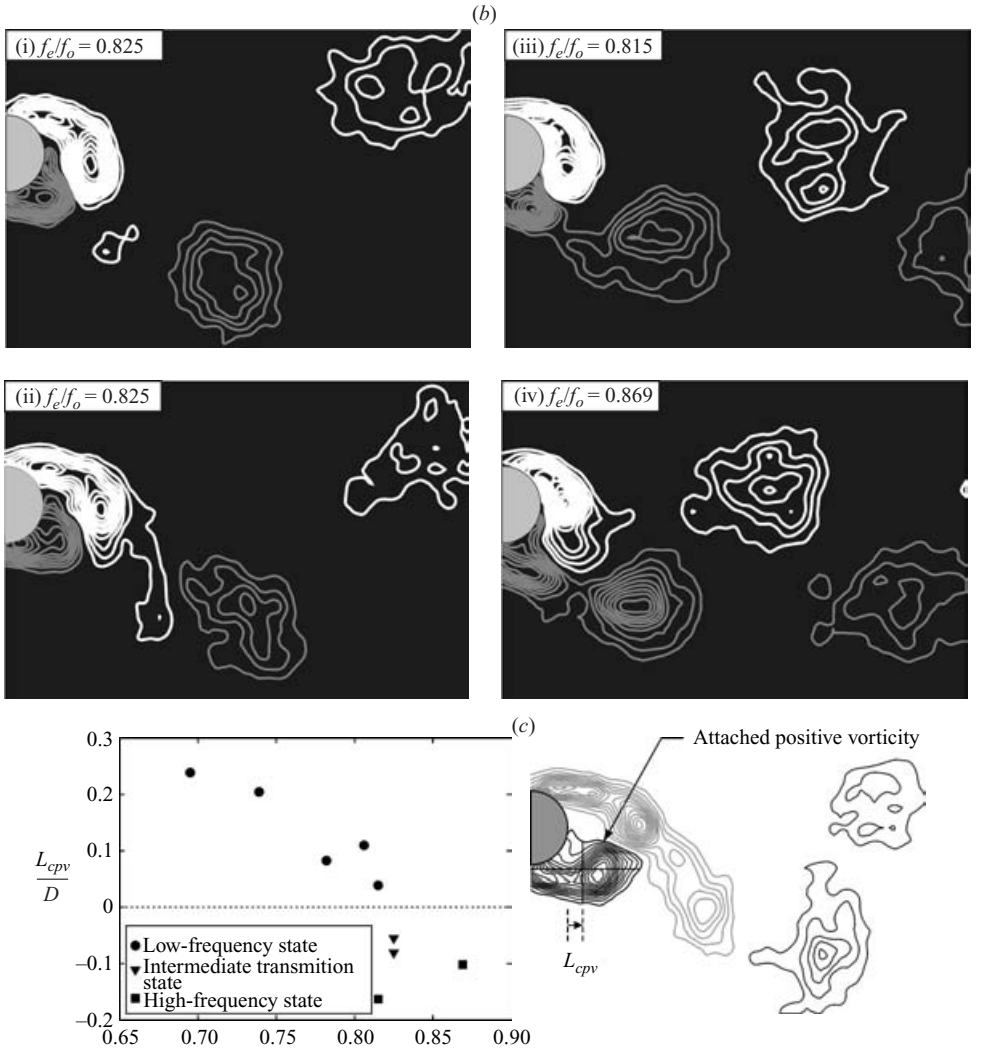

FIGURE 6. (*a*) Phase-averaged vorticity fields showing the variation of wake length with f_e/f_o for the low-frequency state. All images are at the top of the cylinder oscillation. (*b*) Phase-averaged vorticity fields at higher values of f_e/f_o. In images (i) and (ii) the wake appears to be in an intermediate state, while in (iii) and (iv) the wake is in the high-frequency state. (*c*) Variation of the phase-related streamwise position of the centre of attached positive vorticity, L_{cpv} with f_e/f_o and wake state. The schematic on the right-hand side demonstrates the definition of L_{cpv} at the top of the cylinder oscillation.

the long negative vortex structure forms into two structures as it interacts with the positive vorticity in the lower shear layer. As f_e/f_o increases, the wake contracts towards the cylinder and the long negative vortex is pulled further around the back of the cylinder. Also, as f_e/f_o increases, the negative vortex structure, which is about to be shed from the end of the shear layer, becomes progressively weaker, resulting in vortex pairs of unequal strength. Despite the changes in the length of the attached wake and the relative strength within the vortex pairing, both the lift and drag phase remain relatively constant prior to the transition.

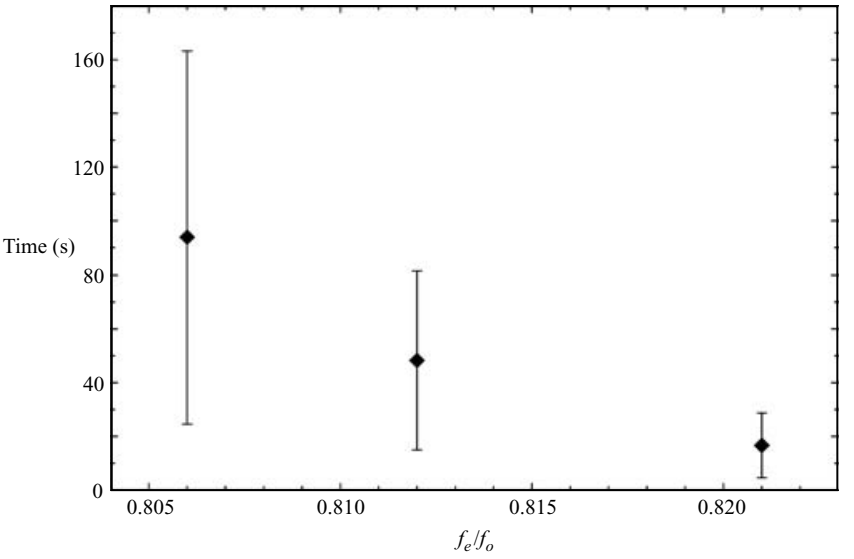

FIGURE 7. Variation of the time from startup to the self-excited transition to the high-frequency state, at $A/D = 0.5$ and $Re = 2300$, where the vertical bars represent one standard deviation.

5.2. *State selection within the transition region*

Within the transition region, it was observed that the system tends to be in one of two stable states: the low- or high-frequency state. In this section, the relative stability of the two states for a specific set of flow parameters is considered. At $A/D = 0.5$ and $Re = 2300$, the self-excited transition was irreversible and transition always occurred from the low-frequency state to the high-frequency state; an example of one such self-excited transition is shown in figure 4(*d*). Within the transition region, when the cylinder starts oscillating its wake state changes from that of a stationary cylinder to the low-frequency state. After a certain period of time, the wake undergoes a self-excited transition to the high-frequency state, which persists indefinitely. Although the wake moves to the low-frequency state immediately after startup, the high-frequency state appears to be more stable. After the self-excited transition, the wake remains indefinitely in the high-frequency state. Thus, within the transition region, the low-frequency state can be interpreted as a state of metastable equilibrium. For the wake to move out of the metastable low-frequency state, a certain level of perturbation is required. As the low-frequency state becomes less stable, the level of perturbation required for a transition will decrease, meaning that at any given instant there is an increased probability that transition will occur. Therefore the average time from startup to transition can be considered to be a measure of the stability of the low-frequency state.

The range of frequencies over which the self-excited transition occurs is quite narrow and at $A/D = 0.5$ and $Re = 2300$ the self-excited transition was observed at only three separate values of f_e/f_o. In figure 7, the average time from startup to transition is plotted as a function of f_e/f_o, where each value was calculated from four to six separate experiments and the vertical bars indicate the standard deviation. As f_e/f_o increases within the transition region, both the average time to transition and the variation in the time to transition clearly decrease. Thus, for the higher frequencies within the transition region, there is a greater probability that the wake will make the

transition to the high-frequency state, indicating that the low-frequency state is less stable.

During the experiments, it was observed that transition could be 'forced' by disturbing the flow upstream of the cylinder. These perturbations were large and unquantified, being induced by oscillating a rod in the channel several metres upstream of the cylinder. It was possible to induce a transition to the high-frequency state at f_e/f_o below the transition frequencies, but after a number oscillations the wake returned to its low-frequency state.

6. Universality of the wake states – variation with amplitude and Reynolds number

Until now the focus has been on the frequency dependence of the wake while holding both the Reynolds number and the amplitude of oscillation constant. The investigation is now extended to examine three values of Reynolds number, $Re = 2300$, 4400 and 9100, and a range of oscillation amplitude, $A/D = 0.25, 0.4, 0.5$ and 0.6. Rather than consider the forces on the cylinder as a function of A/D and Re for a fixed frequency of oscillation, the frequency dependence of the forces at different values of A/D and Re is examined.

In the next section it is shown how the total force on an oscillating body can be broken into two components: a vortex force generated by changes in the wake structure and an apparent mass force. Following this, the variation of the total and vortex forces with A/D and Re is examined. Finally, the nature of the vortex structures in the near wake is discussed. By examining a range of A/D and Re, a number of characteristics that are universal features of this class of flows can be identified.

6.1. *Total and vortex forces*

The analyses of Wu (1981), Noca (1997) and Leonard & Roshko (2001) demonstrated that the total fluid force on a body can be expressed as follows. Using the terminology of Leonard & Roshko (2001),

$$\boldsymbol{F}_{total} = \rho \frac{\mathrm{d}}{\mathrm{d}t} \int_{fluid} \boldsymbol{\omega} \times \boldsymbol{r} \, \mathrm{dV} + \rho A_B \frac{\mathrm{d}\boldsymbol{U}}{\mathrm{d}t} \tag{5}$$

where $\boldsymbol{\omega}$ is the vorticity, $\boldsymbol{r}$ is the distance from the body, A_B is the apparent mass coefficient and $\boldsymbol{U}$ is the velocity of the body.

Without making the assumptions of potential flow, it is possible to demonstrate, via equation (5), that the 'apparent mass' force on a circular cylinder is $-\frac{1}{4}\rho\pi D^2(\mathrm{d}U/\mathrm{d}t)$, as demonstrated by Leonard & Roshko (2001). This expression is valid in the presence of highly separated flow past the cylinder. Govardhan & Williamson (2000) were the first to describe the consequences of force decomposition, into vortex and apparent mass components, in the interpretation of the phase and amplitude of the lift forces on a freely vibrating cylinder. Using the present terminology, in essence, their decomposition is

$$\boldsymbol{F}_{total} = \boldsymbol{F}_{vortex} + \boldsymbol{F}_{am} \tag{6}$$

in which the apparent mass force is given by

$$F_{am}(t) = -\frac{\rho\pi D^2}{4} \frac{\mathrm{d}^2 y}{\mathrm{d}t^2} \tag{7}$$

where $y(t)$ is the displacement of the cylinder, as given by equation (1).

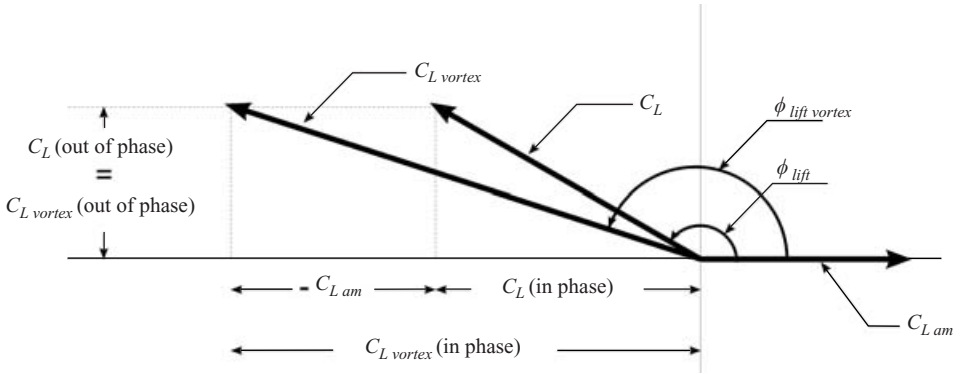

FIGURE 8. Vector diagram showing the relationship between $C_L(t)$ and $C_{L\,vortex}(t)$.

As the cylinder motion is purely transverse, F_{am} has no component in the direction of the drag force and the vortex drag force is equal to the total drag force. The normalized apparent mass force, $C_{L\,am}$, is in phase with the motion of the cylinder and is given by

$$C_{L\,am}(t) = \frac{F_{am}(t)}{\frac{1}{2}\rho U^2 LD} = 2\pi^3 St_o^2 \left(\frac{f_e}{f_o}\right)^2 \frac{A}{D}\sin(\omega t) \tag{8}$$

where St_o is the Strouhal number of the stationary cylinder.

The normalized vortex lift force coefficient $C_{L\,vortex}(t)$ is calculated by subtracting $C_{L\,am}(t)$ from $C_L(t)$, the total lift force coefficient. The vortex lift is now expressed in the same way as the total lift in (2),

$$C_{L\,vortex}(t) \approx C_{L\,vortex}\sin(2\pi f_e t + \phi_{L\,vortex}) \tag{9}$$

where $C_{L\,vortex}$ and $\phi_{L\,vortex}$ are the amplitude and phase of the lift force coefficient due to the vorticity in the wake.

The force properties $C_{L\,vortex}$, $\phi_{L\,vortex}$, C_D, $C_{D\,mean}$ and ϕ_{drag} represent the vortex force on the cylinder and thus can be used to interpret the vorticity field in the wake. For consistency, the symbols ϕ_{lift} and C_L (rather than $\phi_{L\,total}$ and $C_{L\,total}$) will continue to be used to represent the phase and amplitude of the total lift force coefficient. The vector diagram in figure 8 shows the relationships between the phase and amplitude of the total, vortex and apparent mass lift forces. Figure 8 demonstrates an interesting link between the vortex and total lift forces: their out-of-phase components are equal. Thus, as the energy transfer is directly related to the out-of-phase component of the lift force (see § 4.3), it can be expressed in terms of either the total or vortex forces. If the total and vortex lift forces are accurately represented by equations (1) and (2), then the normalized energy transfer is given by

$$C_E \approx \pi\frac{A}{D}C_L\sin(\phi_{lift}) \approx \pi\frac{A}{D}C_{L\,vortex}\ \sin(\phi_{L\,vortex}). \tag{10}$$

6.2. *Total force – variation with A/D and Re*

The compiled data presented in figure 2 show that the simultaneous jump in ϕ_{lift} and C_L at transition occurs for a wide range of Reynolds numbers ($Re = 2300$ to 60 000). Additionally, Staubli's (1983*a*,*b*) data show a similar jump in ϕ_{lift} and C_L for a wide range of $A/D(\approx 0$–$1.0)$. Therefore, the transition appears to be a universal characteristic of the wake for a wide range of A/D and Re.

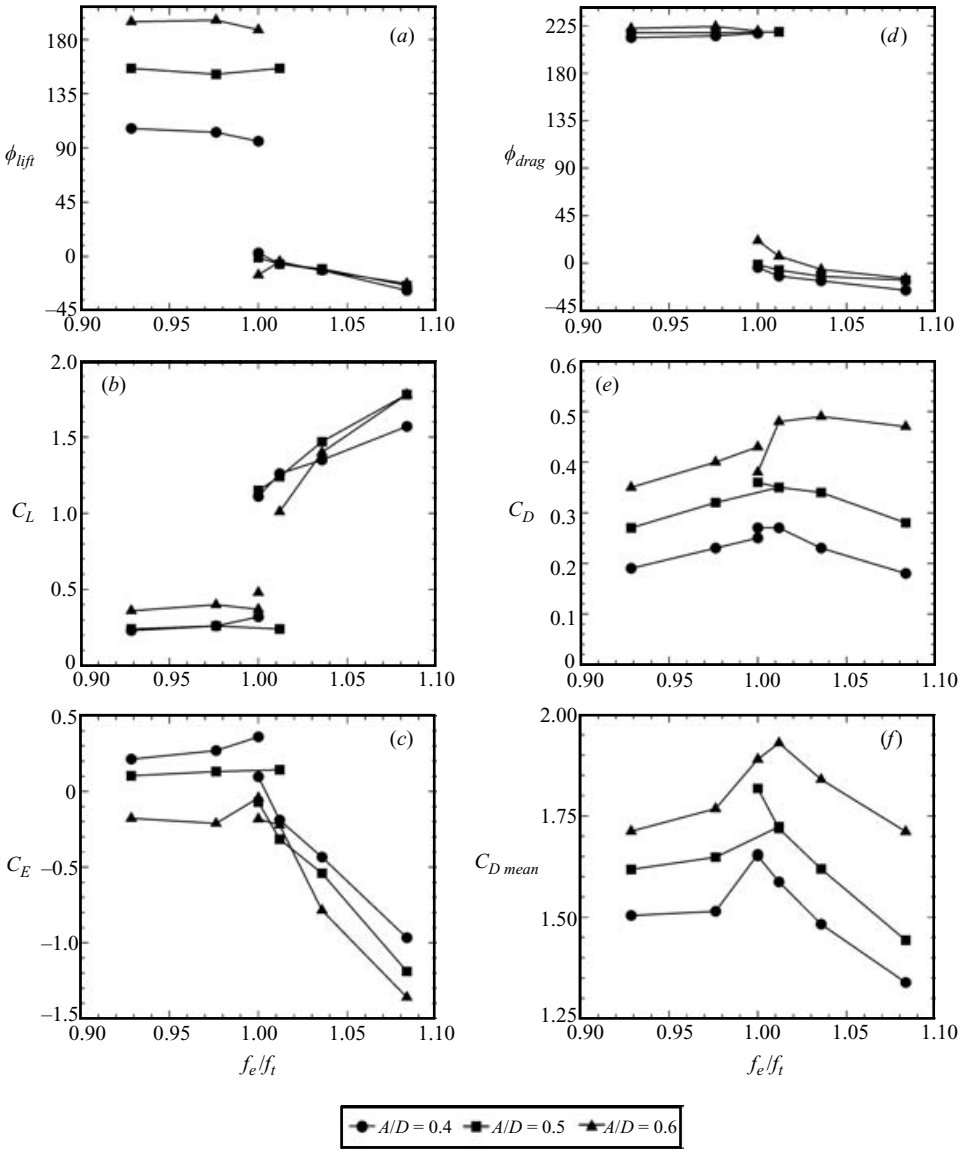

FIGURE 9. For three different oscillation amplitudes ($A/D = 0.4$, 0.5, 0.6) the variation of lift, energy transfer and drag properties with f_e/f_t : (*a*) ϕ_{lift}, (*b*) C_L, (*c*) C_E, (*d*) ϕ_{drag}, (*e*) C_D and (*f*) $C_{D\,mean}$. For all cases $Re = 2300$.

In figure 9 the phase and amplitude of the total lift and drag force coefficients on the cylinder, as well as the energy transfer, are plotted as a function of f_e/f_t for $A/D = 0.4$, 0.5 and 0.6, at $Re = 2300$. These experiments focused on a narrow range of f_e/f_t enclosing the transition region. The trends shown in figure 9 are consistent with those observed as A/D was changed from 0.25 to 0.5 at both $Re = 4400$ and 9100. As A/D increases from 0.4 to 0.6 in figure 9(*a*), there is a large increase in the value of ϕ_{lift} for the low-frequency wake state. At $A/D = 0.4$, the average value of ϕ_{lift} before transition is approximately 102°, whereas at A/D of 0.5 and 0.6 the average values of ϕ_{lift} before transition are 154° and 193° respectively. An A/D increase from

0.5 to 0.6 corresponds to a change in the direction of energy transfer, as illustrated in figure 9(*c*). For the low-frequency state at lower values of A/D positive energy is delivered to the cylinder from the fluid, indicating that an elastically mounted cylinder would oscillate. However, at higher A/D the energy transfer is negative. Intuitively, this makes sense as the oscillations of an elastically mounted cylinder are limited to a certain amplitude, i.e. above a certain amplitude the net energy transfer to the cylinder is no longer positive.

In the high-frequency state, the value of ϕ_{lift} does not vary significantly with A/D. Therefore as A/D increases from 0.4 to 0.6, there is a significant increase in the downwards jump of ϕ_{lift} at transition. At higher Reynolds numbers, Staubli (1983*b*) also found a similar increase in $\Delta\phi_{lift}$ at transition as A/D increased. For frequencies of oscillation close to transition, there was only a small change in the values of C_L as A/D increased from 0.4 to 0.6. However, our data at higher Re and Staubli's previous results suggest that C_L increases with A/D but that this effect is most obvious at higher frequencies, well above transition.

Figures 9(*e*) and 9(*f*) show that both the mean and amplitude of the drag force increase with A/D. For a given wake mode, the vertical displacement of vorticity is directly related to A/D. Therefore, at a constant value of f_e/f_t, as A/D increases there is an increase in the rate at which vorticity is displaced vertically. Referring again to equation (5), the increase in C_D is consistent with an increase in the rate of change of the vertical vorticity moment, i.e. an increase in the rate at which vorticity moves vertically. As A/D increases, there is also a net increase in the vertical movement of vorticity, which corresponds to a higher mean drag.

Over the range of A/D studied, the frequency at which transition occurred did not change significantly. However, there was a change in the nature of the self-excited transition. At $A/D = 0.4$ and 0.5, there was a non-reversible self-excited transition from the low-frequency state to the high-frequency state which was consistent with the self-excited transition discussed previously. At $A/D = 0.6$, a self-excited transition was also initiated from the low-frequency state, but at $f_e/f_o = 0.841$, the forces on the cylinder after the transition were not fully consistent with the high-frequency state.

The manner in which Re affects the wake of an oscillating cylinder is complex, as shown in figure 2, where C_L and ϕ_{lift} are plotted at $A/D = 0.5$ for a wide range of Re: 2300–60 000. In particular, the non-dimensional frequency, f_t/f_o at which the transition from the low- to high-frequency state occurs varies in an apparently non-systematic fashion with Re. The reasons for this variation are at this stage not well understood. Additionally, when comparing results from different experimental facilities in figure 2, it is difficult to fully consider the way in which other factors, such as the level of free-stream turbulence and the method of changing f_e/f_o, affect the trends in the force data. The results from the current experiment in figure 10 show the frequency dependence of the total lift force, drag force and the energy transfer for three different Re: 2300, 4410 and 9100, where for all cases $A/D = 0.5$. The main focus of figure 10 is the variation of the forces with Re for the two different wake states; therefore the results were plotted against f_e/f_t rather than f_e/f_o, where (Re, f_t/f_o) = (2300, 0.826); (4410, 1.021); (9100, 1.000).

Figure 10(*a*) shows that, as Re increases, there is a systematic increase in the value of ϕ_{lift} for the low-frequency wake state. Therefore, as for A/D, increasing Re can change the direction of energy transfer of the low-frequency state. As shown in figure 10(*c*), at $Re = 2300$ there is a small positive energy transfer to the cylinder but for the higher Re the energy transfer is negative. For the high-frequency state ϕ_{lift} becomes more negative as Re increases. When, as in figure 10(*a*), the transition from

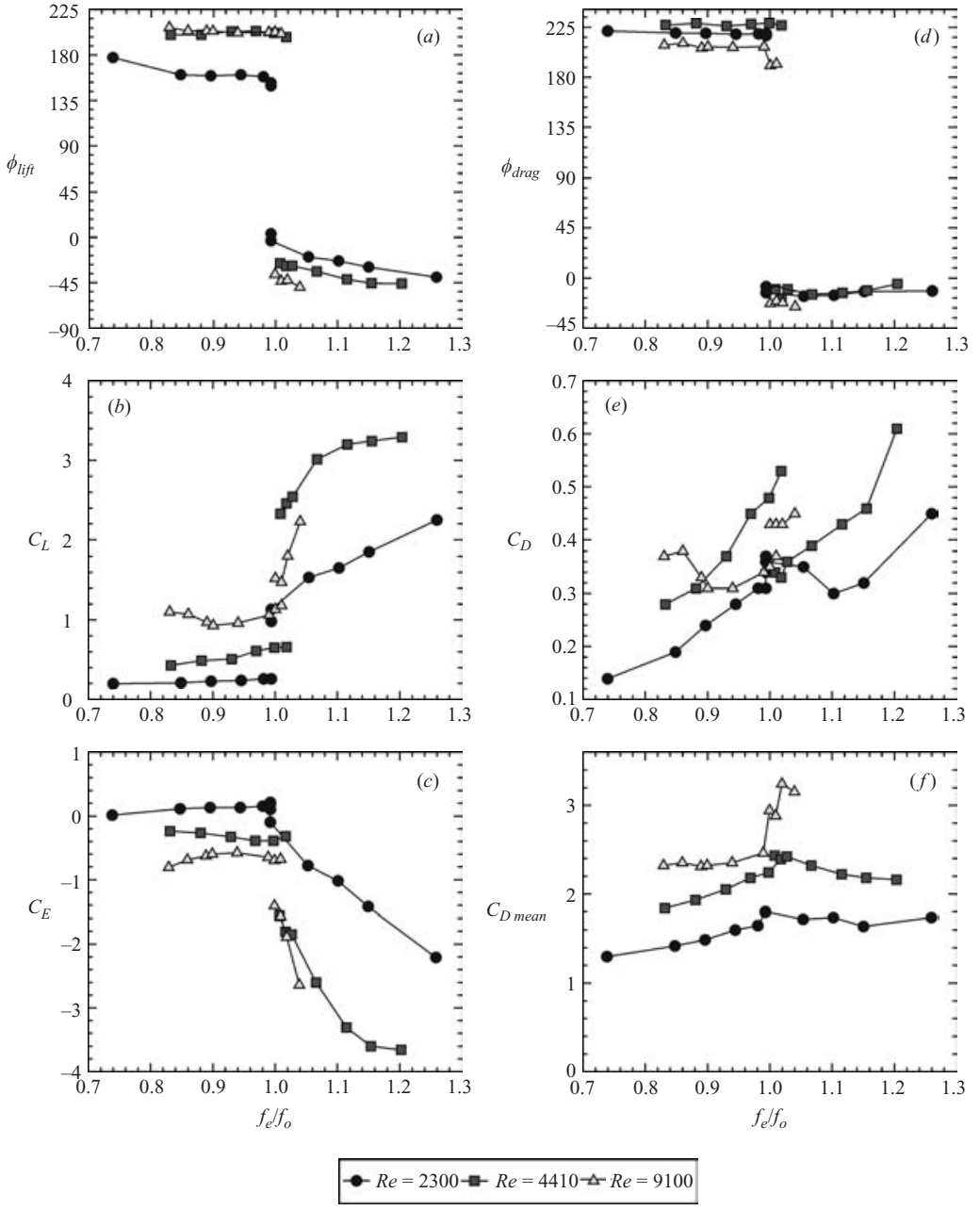

FIGURE 10. For three different Reynolds Numbers (Re = 2300, 4410, 9100) the variation of lift, energy transfer and drag properties with f_e/f_o: (*a*) ϕ_{lift}, (*b*) C_L, (*c*) C_E, (*d*) ϕ_{drag}, (*e*) C_D and (*f*) $C_{D\,mean}$. For all cases $A/D = 0.5$.

the low- to high-frequency states is plotted as a phase jump in the clockwise direction the magnitude of the jump in ϕ_{lift} appears to increase as Re increases. If, however, the transition were plotted as a phase jump in the anti-clockwise direction, i.e. the values for the high-frequency state are plotted in the quadrant between 270° and just above

360°, ϕ_{lift} would increase with increasing Re for both the low- and high-frequency states and the phase jump at transition would be relatively similar for all Re.

Figure 10(b) shows that, for the low-frequency state, the amplitude of the total fluctuating lift force increases as Re increases from 2300 to 9100. For both $Re = 2300$ and 4410 the transition between the low- and high-frequency states corresponds to a distinct jump in C_L. At $Re = 9100$ the transition corresponds to a relatively small jump in C_L, but following the transition to the high-frequency state C_L increases rapidly. Both the energy transfer and the mean drag force, shown in figures 10(c) and 10(f) respectively, vary systematically as Re increases from 2300 to 9100. For both the low- and high-frequency states, as Re increases C_E becomes more negative, while $C_{D\,mean}$ increases. The variation of C_D with Re in figure 10(e) is complicated and a trend in C_D is not entirely clear. The phase of the drag force, shown in figure 10(d), shows relatively little variation with Re and the values of ϕ_{drag} are very similar to those in figure 9(d). The behaviour of the force properties in figure 10 is consistent with observations at the smaller oscillation amplitude of $A/D = 0.25$ as Re increased from 4410 to 9100.

The most striking feature of the force and energy plots in figure 9 and figure 10 is that while $\phi_{lift}, C_L, C_E, C_D$ and $C_{D\,mean}$ all show significant, and generally systematic, variations with A/D and Re, the phase of the drag force does not vary significantly with A/D and Re but appears to depend primarily on wake state. The drag force is a vortex force and therefore ϕ_{drag} is related to the phase of the movement of vorticity in the wake; ϕ_{lift} is the phase of the total lift force and therefore does not directly relate to the phase of vorticity movement in the wake. In the next section the vortex lift forces on the cylinder are considered.

Closer examination of the transition region also showed that, for $A/D = 0.5$, the characteristics of the self-excited transition at $Re = 9100$ are very different from those at lower values of Re. In this case, the self-excited transition occurred from the high-frequency state to the low-frequency state, i.e. in the opposite direction from the self-excited transition at lower Re. Following our discussion of relative stability in § 5.2, the 'reverse' transition at $Re = 9100$ indicates that in this case the wake preferred to move from the stationary cylinder state to a meta-stable high-frequency state. This represents a change in the relative stability of the stationary, low- and high-frequency wake states. Variation of the relative stability of the wake states with Re (or A/D) is consistent with changes in the value of f_t/f_o.

6.3. *Vortex force – collapse of vortex lift and drag phase*

The effect of oscillation amplitude and Reynolds number on the vortex force will now be examined. To recap, the vortex force is the force due to the movement of vorticity, i.e. the force due to the wake, and is calculated by subtracting the apparent mass force from the total force. The apparent mass force, F_{am}, is inline and inphase with the transverse oscillation of the cylinder. Therefore, as shown in figure 8, subtracting F_{am} only changes the in-phase component of the lift force; the drag force and the out-of-phase component of the lift force are unchanged. This means that subtracting F_{am} will not change the direction or magnitude of the energy transfer between the cylinder and the fluid.

In figures 11(a) and 11(c) ϕ_{lift} and $\phi_{L\,vortex}$ are plotted for a number of experiments where A/D varied from 0.25 to 0.6, and Re varied between 2300 and 9100. As discussed previously, for the low-frequency state, ϕ_{lift} varies with both A/D and Re; however, when F_{am} is subtracted the low-frequency vortex lift phase in figure 11(c) collapses towards $\phi_{L\,vortex} = 180°$. As the out-of-phase components of the total and

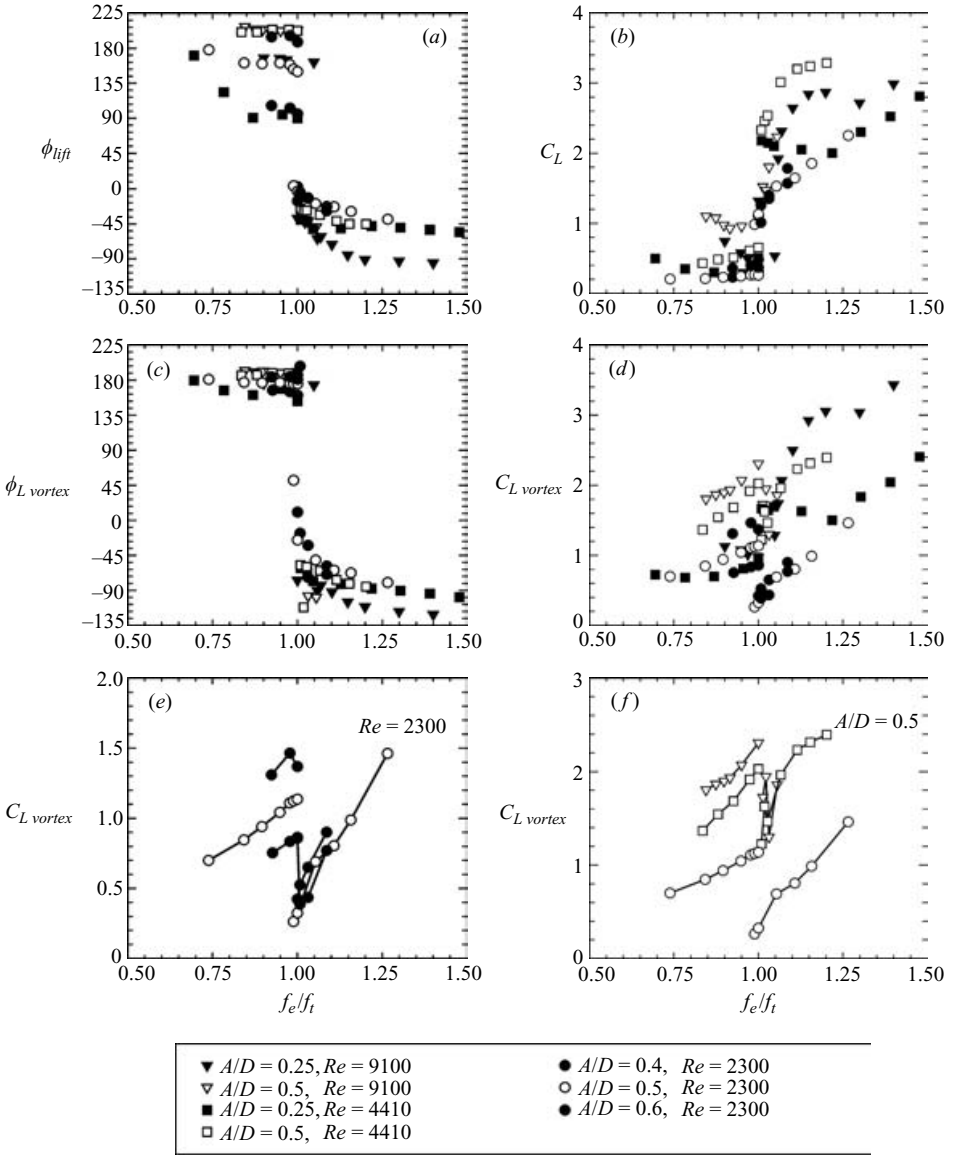

FIGURE 11. (*a*) ϕ_{lift}, (*b*) C_L, (*c*) $\phi_{L\,vortex}$ and (*d*) $C_{L\,vortex}$ versus f_e/f_t for a range of A/D and Re, demonstrating the effect of subtracting the apparent mass force. $C_{L\,vortex}$ is replotted for (*e*) a range of A/D at $Re = 2300$, and (*f*) a range of Re at $A/D = 0.5$.

vortex lift forces are equal, see figure 8, subtracting F_{am} cannot cause the lift phase to move through either 180° or 0°. However, subtracting F_{am} can cause large changes in lift phase and the difference between $\phi_{L\,vortex}$ and ϕ_{lift} can be up to 180°. Immediately following the transition to the high-frequency state there is an increase in the scatter of $\phi_{L\,vortex}$. The main source of this scatter is that for $A/D = 0.4$ and 0.5 immediately following transition $\phi_{L\,vortex}$ tends to be close to 0°, decreasing smoothly towards −90° as f_e/f_o increases further, whereas for $A/D = 0.25$ and 0.6 at the transition to the high-frequency state $\phi_{L\,vortex}$ tended to jump straight down to −90°.

While subtracting F_{am} caused the lift phase to collapse towards a single set of values, the scattered nature of the $C_{L\,vortex}$ values in figure 11(d) shows that the same is not true for the lift amplitude. Over a range of A/D and Re values, the variation of C_L with f_e/f_t, shown in figure 11(b), maintains the same general form: C_L is small and relatively constant for the low-frequency state, the transition to the high-frequency state corresponds to a jump in C_L and for the high-frequency state C_L increases with increasing f_e/f_t. Examination of figure 11(d) shows that, in general, $C_{L\,vortex}$ increases with f_e/f_t for both the low- and high-frequency wake states, with a discontinuity or jump at transition. However, over a range of A/D and Re there is significant variation in the magnitude of $C_{L\,vortex}$ as well as the direction of the jump in $C_{L\,vortex}$ at transition.

Figure 11(e) shows the variation of $C_{L\,vortex}$ with A/D at a constant Reynolds number of 2300. For the low-frequency state, $C_{L\,vortex}$ increases markedly with A/D but for the high-frequency state, particularly close to transition, there is little variation in $C_{L\,vortex}$ with A/D. In figure 11(e) $C_{L\,vortex}$ jumps downwards at transition and the magnitude of this jump decreases as A/D gets smaller. If this trend continues then for even smaller values of A/D $C_{L\,vortex}$ will actually jump upwards at transition. This is in fact what happens at $A/D = 0.25$, shown in figure 11(d), where for Re of both 4410 and 9100, represented by the black squares and triangles respectively, the transition from the low- to high-frequency state corresponds to an upwards jump in $C_{L\,vortex}$. The variation of $C_{L\,vortex}$ with Re is shown in figure 11(f), where $C_{L\,vortex}$ is plotted for a range of Reynolds numbers at a constant oscillation amplitude of $A/D = 0.5$. As Re increases from 2300 to 9100 there is an upwards shift in the amplitude of the vortex force for both the low- and high-frequency wake states. As Re increases from 4410 to 9100 for the high-frequency state the increase in $C_{L\,vortex}$ close to the transition region is very small. However, as discussed by Carberry (2002), data obtained at other values of AD suggests that at higher oscillation frequencies the magnitude of the increase in $C_{L\,vortex}$ as Re increases from 4410 to 9100 will be larger.

In figures 9, 10, and 11, the phases of the vortex lift and drag forces are plotted for cases where either A/D or Re varied. In all cases it was shown that $\phi_{L\,vortex}$ and ϕ_{drag} did not vary significantly with A/D or Re. In figure 12 values of $\phi_{L\,vortex}$ and ϕ_{drag} resulting from all our experiments, A/D (0.25–0.6) and Re (2300–9100), are plotted as a function of f_e/f_t on a single axis. Over this parameter set, figure 12 demonstrates the striking collapse of $\phi_{L\,vortex}$ and also of ϕ_{drag} towards constant values for a given wake state. The fact that the values of $\phi_{L\,vortex}$ and ϕ_{drag} do not vary significantly with A/D and Re indicates that the timing of vortex shedding is relatively independent of these parameters. This is confirmed by the vorticity fields in figure 13 and figure 14, which will be discussed in the next section.

C_D and $C_{L\,vortex}$ do not collapse towards a single value for a given wake state, indicating that while the timing of vortex shedding is approximately constant, the level and distribution of vorticity depends on both Re and A/D. Moreover, unlike the phase of the vortex lift and drag forces further away from the transition region, the amplitude of the fluctuating vortex lift and drag forces, $C_{L\,vortex}$ and C_D, tend to increase with the frequency of oscillation.

6.4. *Vorticity fields*

The phase-averaged vorticity fields at $A/D = 0.25, 0.4, 0.5$ and 0.6 are shown in figures 13 and 14 for the low- and high-frequency wake states respectively. The Reynolds number is 9100 for $A/D = 0.25$, while at larger amplitudes, $A/D = 0.4, 0.5$, and 0.6, $Re = 2300$. The low-frequency wake modes in figure 13 are shown as the

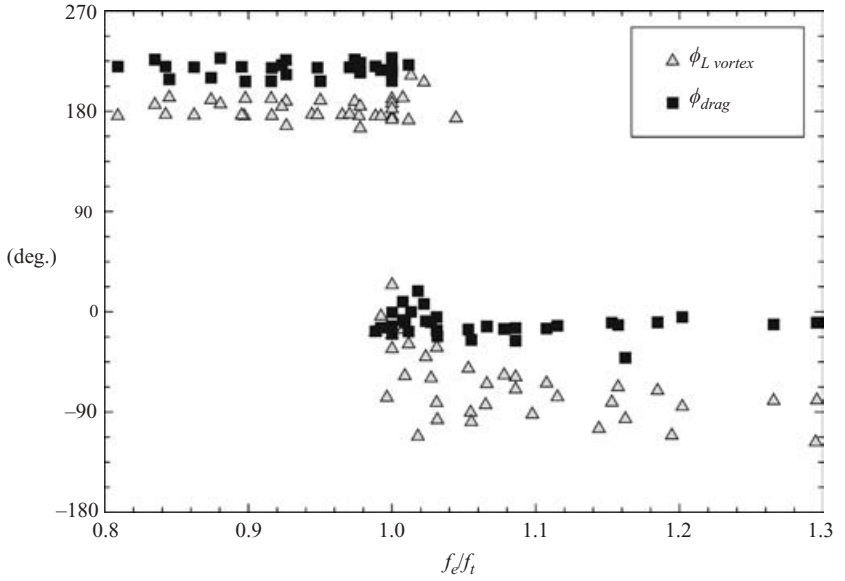

FIGURE 12. Phase of the vortex lift and drag forces, $\phi_{L\,vortex}$ and ϕ_{drag} for all experiments with A/D ranging from 0.25 to 0.6 and Re ranging from 2300 to 9100.

cylinder moves through its downwards stroke. Looking down the columns, at the same phase point in the oscillation, allows comparison of the wakes at different A/D, whereas looking along the rows shows the wake development as the cylinder moves through its downward stroke.

At the top of the cylinder oscillation, the low-frequency wake in figure 13 (column i) has an attached negative shear layer that extends across the base of the cylinder into the lower half of the wake. As A/D increases from 0.25 to 0.6, there is a clear increase in the length of the attached shear layer. At $A/D = 0.5$ and 0.6, as the cylinder moves through the downward stroke in columns (ii) and (iii) a portion of vorticity separates from the end of the longer shear layers and the negative vorticity is shed as two separate structures, resulting in the formation of the 2P mode of shedding. At $A/D = 0.4$ the negative vorticity is shed as a single band which shows a propensity to break into two separate structures. However, at $A/D = 0.25$ the attached shear layer is much shorter, only just extending past the bottom of the cylinder, and a portion of vorticity does not separate from the end of the shear layer. Therefore, while the other features of the low-frequency wake state persist at small values of A/D, there appears to be a limiting amplitude, below which the shear layer is not long enough to generate the 2P mode of shedding. As the cylinder moves through its downward stroke, the lower (positive) shear layer forms a distinct upwards angle. Examination of the vorticity fields in column (iii) at the point of maximum vertical velocity shows a clear increase in the angle of the wake as A/D increases.

As A/D varies from 0.25 to 0.6, the general structure of the low-frequency wakes in figure 13 is very similar; however there are systematic changes in the location and extent of the vortex structures in the near wake as A/D increases. Importantly, at each point in the cylinder displacement cycle, i.e. each column in figure 13, the low-frequency wakes are essentially at the same point in their shedding cycle and the timing of vortex shedding is effectively independent of A/D and Re.

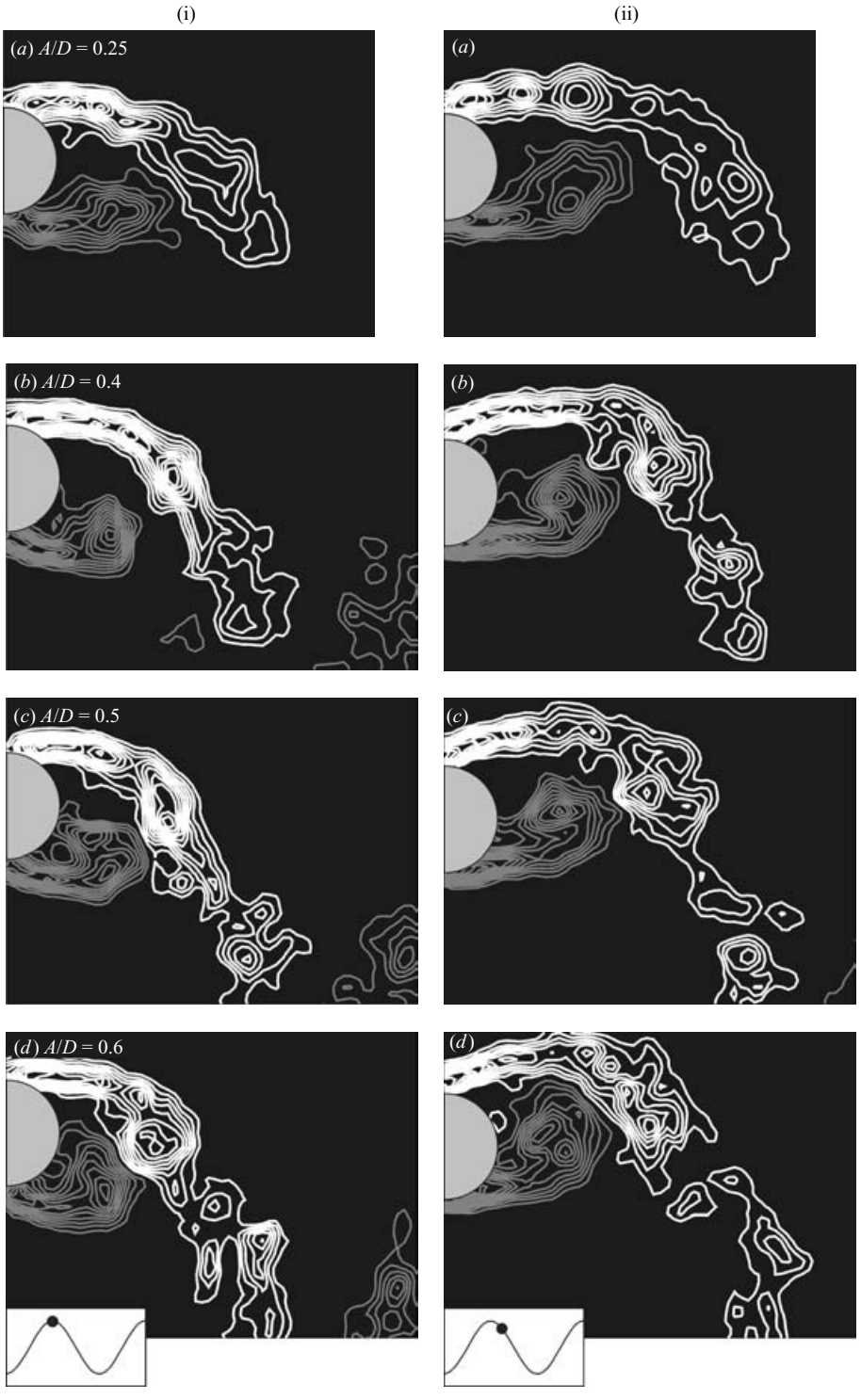

FIGURE 13(i, ii). For caption see facing page.

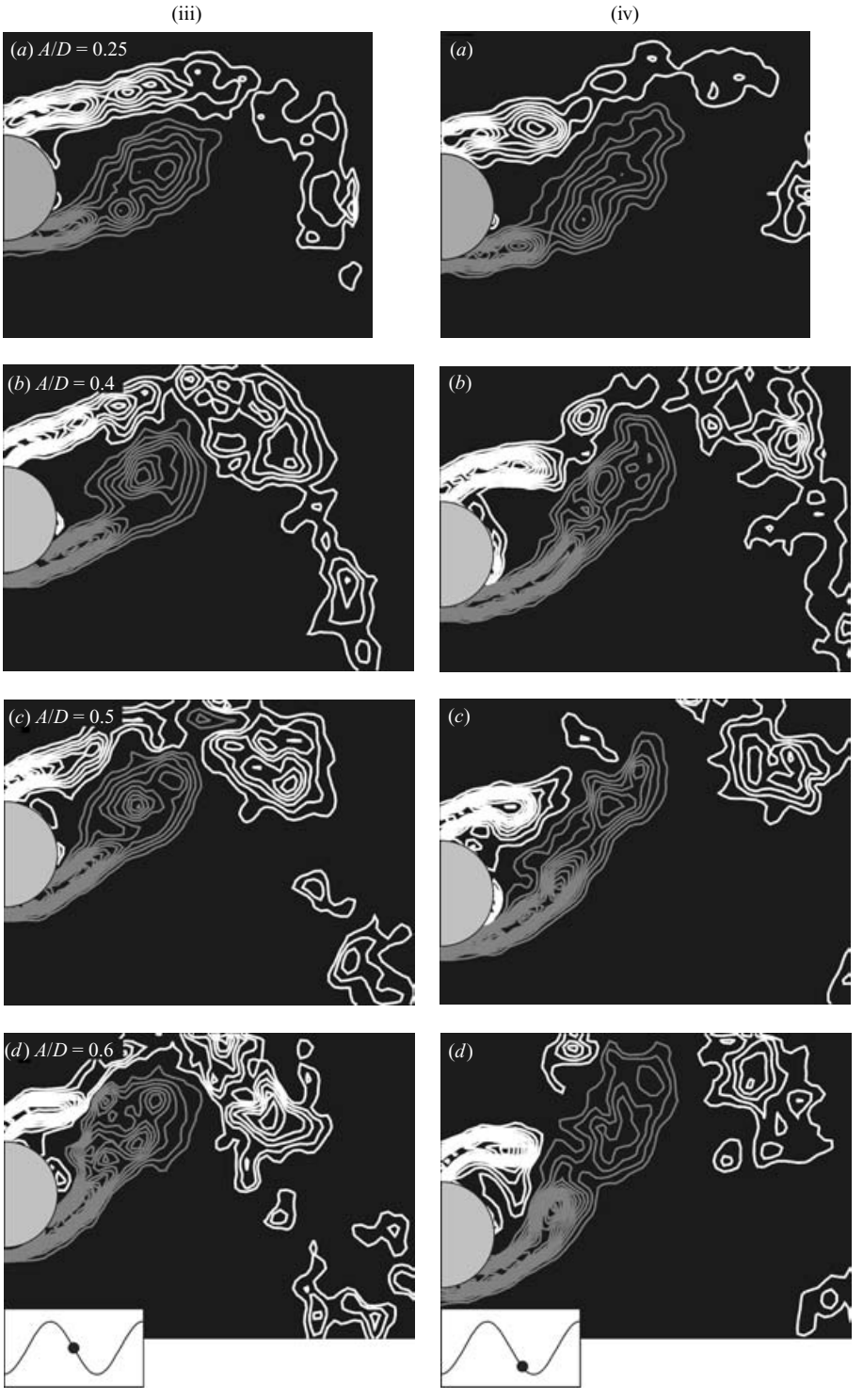

FIGURE 13. Phase-averaged low-frequency state vorticity fields for (*a*) $A/D = 0.25$ ($Re = 9100$, $f_e/f_t = 0.962$) and (*b*) $A/D = 0.4$, (*c*) $A/D = 0.5$ and (*d*) $A/D = 0.6$ all at $Re = 2300$ and $f_e/f_t = 0.978$. As indicated by the displacement inserts the images were acquired at evenly spaced intervals such that (i) is at the top of the cylinder oscillation and (iii) is at the mid point of the downwards stroke.

Figure 14 shows the high-frequency wake states captured at the top of the oscillation cycle. As for the low-frequency wake state, the timing and mode of the vortex shedding are essentially the same as A/D increases from 0.25 to 0.6, at Re of 2300 and 9100. As A/D and Re change, the differences in the distribution of the vorticity for the high-frequency wakes in figure 14 are quite subtle due to the condensed nature of the wakes. As A/D is increased the vorticity breaks up quickly as it moves downstream. Additional images over a range of Re for $A/D = 0.5$ indicate that there is a similar increase in the breakup of vorticity at higher Re.

For a particular wake state, the robustness of the phase of vortex shedding indicates that the shedding is phase locked to the displacement of the cylinder. The relatively constant values of $\phi_{L\,vortex}$ and ϕ_{drag} in each wake state, shown in figure 12 for a range of A/D and Re, are consistent with the constant phase and mode of vortex shedding illustrated in figure 13 and figure 14. While the timing and mode of vortex shedding appear to be independent of A/D and Re, there are systematic variations in the distribution of vorticity in the near wake. The changes in the distribution of vorticity are consistent with the fact that in figure 11(d) there is significant variation in the amplitude of the vortex lift force; however it is difficult to directly relate the changes in $C_{L\,vortex}$ to the changes in the distribution of vorticity.

7. Variation of wake frequencies with f_e/f_o

An elastically mounted cylinder vibrates at a frequency that depends on the reduced velocity, wake state and the properties of the structure incorporating the cylinder, including the structural spring constant, structural damping and mass. However, once a particular structure has been selected, the natural frequency of the structure is constant during the experiment. When the oscillations are forced, the situation is reversed: the forcing controls the frequency of oscillation but the frequency of the wake's natural instability varies with f_e and wake state.

In figure 15, the lift spectra for a range of oscillation frequencies, at $A/D = 0.25$ and $Re = 4410$, are presented on a single three-dimensional plot. Typically, the lift spectra have a strong peak at f_e, the frequency of oscillation, with a second, smaller peak at a frequency f_{nos}, where f_{nos} is not a harmonic or sub-harmonic of f_e. The value of f_{nos} is close to, but not necessarily equal to, f_o, the natural Kármán frequency of the stationary cylinder and it appears that f_{nos} is associated with the natural frequency of the oscillating wake. The distribution of energy between the peaks at f_e and f_{nos} depends on the response of the wake to the cylinder motion and is often used to determine the synchronization or lock-in region. As the wake moves beyond the lock-in region f_{nos} becomes the dominant frequency in the wake. The variation in the lift spectra with f_e/f_o in figure 15 is similar to that observed by Szechenyi & Loiseau (1975) at much higher Reynolds numbers.

For the range of frequencies shown in figure 15, the wake is always locked onto the cylinder oscillations and the peak at f_{nos} is generally much smaller than the peak at f_e. For the lower frequencies of oscillation, however, both peaks are small and of comparable energy levels. As f_e/f_o increases the energy at f_{nos} decreases and there is a gradual increase in the energy at f_e, until at transition there is a sharp increase in the energy at f_e. The jump in the energy at the oscillation frequency corresponds to the jump in the amplitude of the total lift force shown in figure 11(b). At frequencies just above transition the second peak at f_{nos} could not be resolved. However, as f_e/f_o increases further the second peak at f_{nos} reappears.

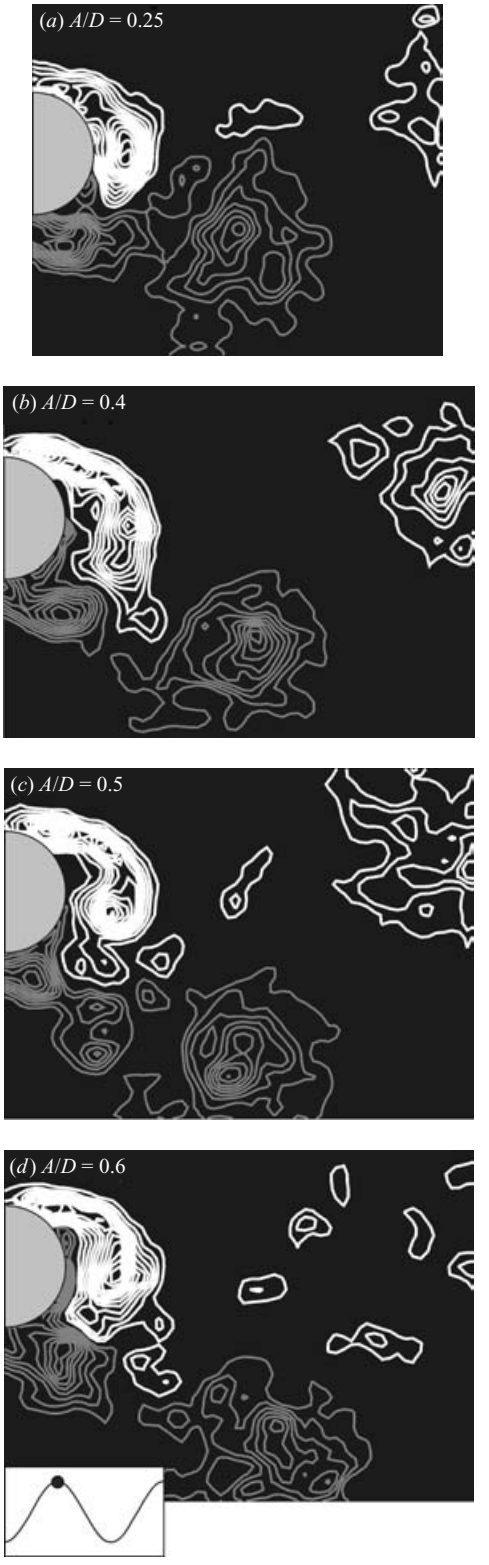

FIGURE 14. Phase-averaged high-frequency state vorticity fields for (*a*) $A/D = 0.25$ at $Re = 9100$ and (*b*) $A/D = 0.4$, (*c*) $A/D = 0.5$ and (*d*) $A/D = 0.6$ all at $Re = 2300$.

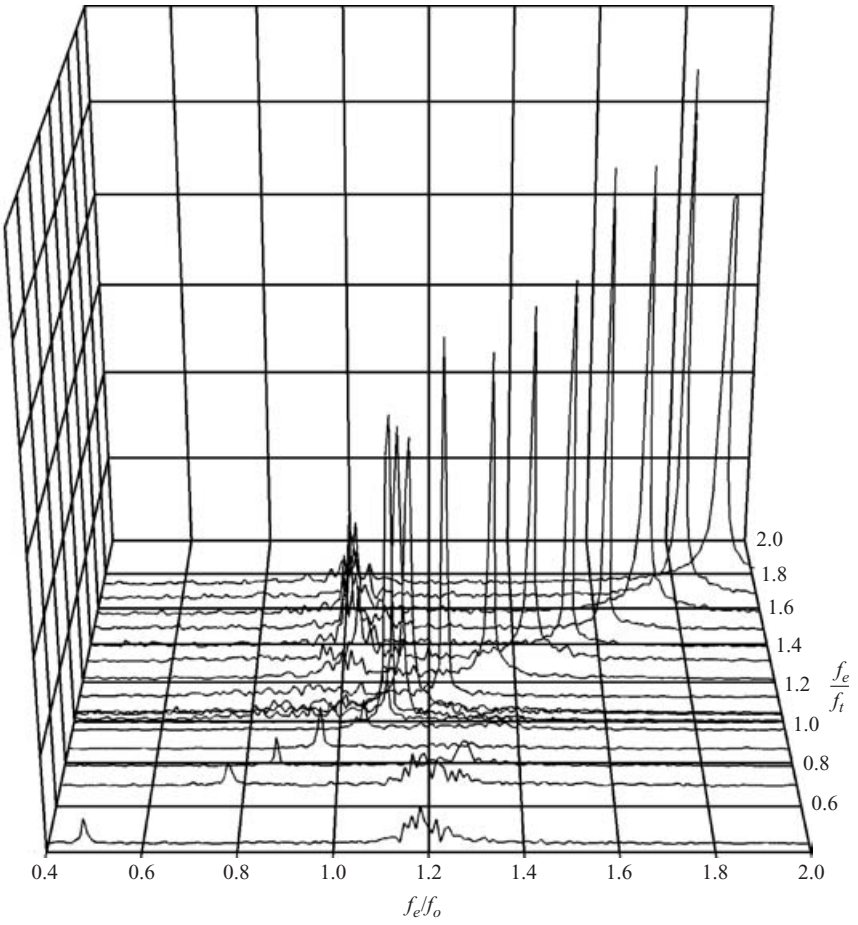

FIGURE 15. Variation of lift spectra with oscillation frequency f_e/f_t at $A/D = 0.25$ and $Re = 4410$.

In figure 16, the frequencies of the spectral peaks in figure 15, f_{nos}/f_o, f_e/f_o and f_e/f_{nos} are plotted against the normalized oscillation frequency. For all frequencies of oscillation, the natural frequency of the oscillating wake is greater than the natural frequency of the stationary wake, i.e. $f_{nos}/f_o > 1$. As the frequency of oscillation increases towards transition ($f_e/f_t \rightarrow 1$) both f_e and f_{nos} increase; however the relative rates of increase are such that the peaks, represented in figure 16 by the solid circles and the open triangles respectively, move closer together. Prior to transition, f_{nos} is greater than f_e, with transition occurring before the peaks intersect. Immediately following transition, f_{nos} could not be resolved; however for $f_e/f_t \geqslant 1.2$, f_{nos} is slightly greater than f_o and does vary significantly with f_e/f_t. Therefore, after transition f_{nos} is less than f_e and the peaks move apart as the frequency of oscillation increases.

At transition, there is a downward jump in f_{nos}, which is consistent with the corresponding change in the mode of vortex shedding. Additionally, the transition between the two wake states corresponds to a change in the relationship between the forcing frequency and the natural frequency of the oscillating wake. When the wake is locked onto the forced oscillations vortex shedding occurs at the forcing frequency, f_e. At low frequencies, prior to transition, f_{nos} is greater than f_e, indicating that

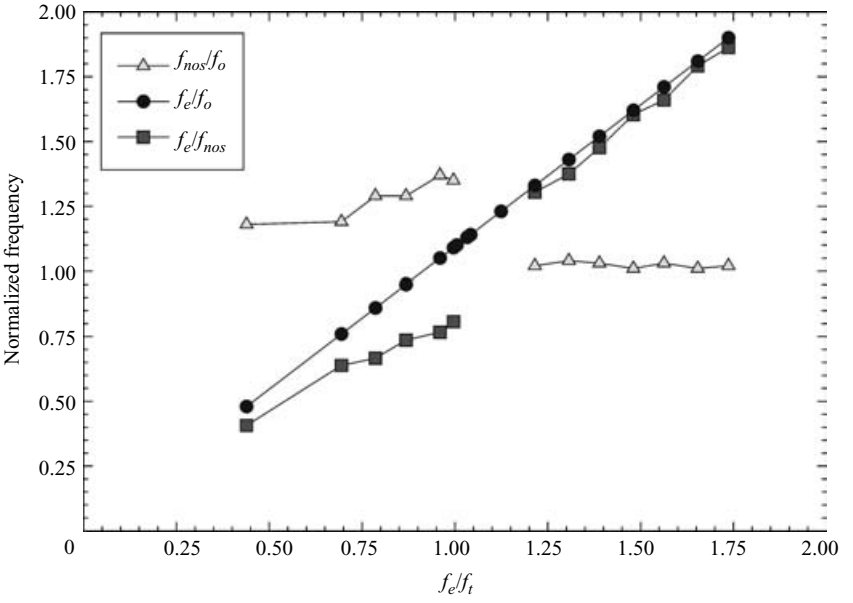

FIGURE 16. Variation of the most energetic frequencies in the lift spectra with f_e/f_t at $A/D = 0.25$ and $Re = 4410$. The corresponding spectra are shown in figure 15.

shedding controlled by the natural instability would occur faster than 'allowed' by the forced oscillation. The resulting wake mode forms long extended shear layers. As f_e/f_o increases the peaks at f_{nos} and f_e move together and the wake contracts. After transition the natural frequency is less than the forcing frequency ($f_{nos} < f_e$) and as f_e/f_o increases the peaks move further apart. Thus, the forced vortex shedding occurs faster than it would if shedding were controlled by the natural instability of the wake. In this case, the wake is significantly shorter and the mode of vortex shedding is different.

8. Comparison of forced and freely oscillating cylinders

This section considers the relationship between a cylinder forced to oscillate at frequencies close to the natural frequency of the wake and the free oscillations of an elastically mounted cylinder. The relationship between these two cases has proved surprisingly complicated. However, our results show that many of the fundamental features of the free and forced cases are in fact strikingly similar.

In order to establish this equivalence, it is necessary to define the branches of response of the freely oscillating cylinder, relative to the present low- and high-frequency states. Feng (1968) showed that when the amplitude of the cylinder oscillation is plotted against reduced velocity, U^*, there are at least two different response branches. As the free-stream velocity is increased through $U^* = 5.0$ ($f \approx f_o \approx f_{struc}$) there is a change in both the amplitude of oscillation and the phase of the lift force as the wake moves to a different branch. Brika & Laneville (1993), in an investigation of the response of a long cable to transverse flow, showed there is a link between these branches, the structures of the wake and the vortex phase angles. Subsequent investigations of an elastically mounted cylinder by Khalak & Williamson (1999) and Govardhan & Williamson (2000) confirmed that the different

branches correspond to different wake structures and that there are sharp jumps in the lift phase and amplitude as the wake moves between branches. Khalak & Williamson (1999) also showed that the number of response branches varied with $m^*\zeta$, the mass damping parameter of the cylindrical structure. At higher values of $m^*\zeta$, such as those investigated by Feng (1968), there are two response branches: the lower and initial. However, at very low value of $m^*\zeta$ there is a third upper branch where the cylinder oscillates at very high amplitudes. Khalak & Williamson (1999) showed that the velocity dependence is best described by a normalized reduced velocity, $(U^*/f^*)St_o$, where $U^* = U/(f_{struc}D)$, $f^* = f/f_{struc}$ and $St_o = f_oD/U$, as when the amplitude response is plotted against $(U^*/f^*)St_o$ there is a good collapse of the lower and initial branches for a wide range of m^*.

For an elastically mounted cylinder, varying the reduced velocity changes f_o/f_{struc}, the ratio of the natural frequency of the stationary wake to the structural frequency. Thus, if f, the frequency of oscillation for an elastically mounted cylinder, is considered to be equivalent to f_e, the frequency at which the forced cylinder oscillates, the parameter $(U^*/f^*)St_o$ is inversely equivalent to f_e/f_o. Although it appears obvious that we can correctly equate f and f_e for the forced and free oscillations the oscillation frequencies of the cylinder have different physical meanings: f is the frequency at which the freely oscillating cylinder responds to periodic forcing from the wake, whereas f_e is the frequency at which the forced motion of the cylinder perturbs the wake.

For a cylinder undergoing forced oscillations, as f_e/f_o passes through unity there is a transition between the low- and high-frequency states. Additionally, for oscillation frequencies within the transition region, at a constant frequency of oscillation the wake can undergo a non-reversible, self-excited transition between the low- and high-frequency wake states. Similarly, for a freely oscillating cylinder there is a transition between different response branches as the reduced velocity is varied. Brika & Laneville (1993) also observed a self-excited transition when a cable undergoes vortex-induced vibration at certain constant reduced velocities. However, the self-excited transition was only observed when the cable was subject to large-scale oscillations prior to being released, and did not occur when the cylinder was released from rest. The self-excited transition of the cable took a long time to develop, often taking more than 1000 oscillations, and the amplitude of oscillation changes gradually during the transition. This contrasts with the results for a cylinder forced to oscillate at a constant amplitude, where the self-excited transition occurred in less than 50 oscillations. Khalak & Williamson (1999) found that elastically mounted cylinders could switch intermittently between two response branches. This was shown using the lift phase, which they found to be a direct indicator of the predominant mode of oscillation.

Figure 17 compares the structure of the near wake for the forced and freely oscillating cylinders for two sets of similar flow and oscillation parameters (f_e/f_o or $(U^*/f^*)St_o$, A/D and Re), where in all cases the wakes are shown when the cylinder is positioned at the top of its oscillation cycle. The vorticity fields in figures 17(b) and 17(d), reproduced from Govardhan & Williamson (2000), show the structure of the near wake for the lower and initial response branches of the freely oscillating cylinder. For the case where the motion is forced figures 17(a) and 17(c) show the wake structures for the low- and high-frequency states.

Figures 17(a) and 17(b) show that at the same oscillation amplitude of $A/D = 0.6$ the structure of the near wake for the low-frequency state and the lower response branch are almost identical, and in both cases the mode of vortex shedding is clearly

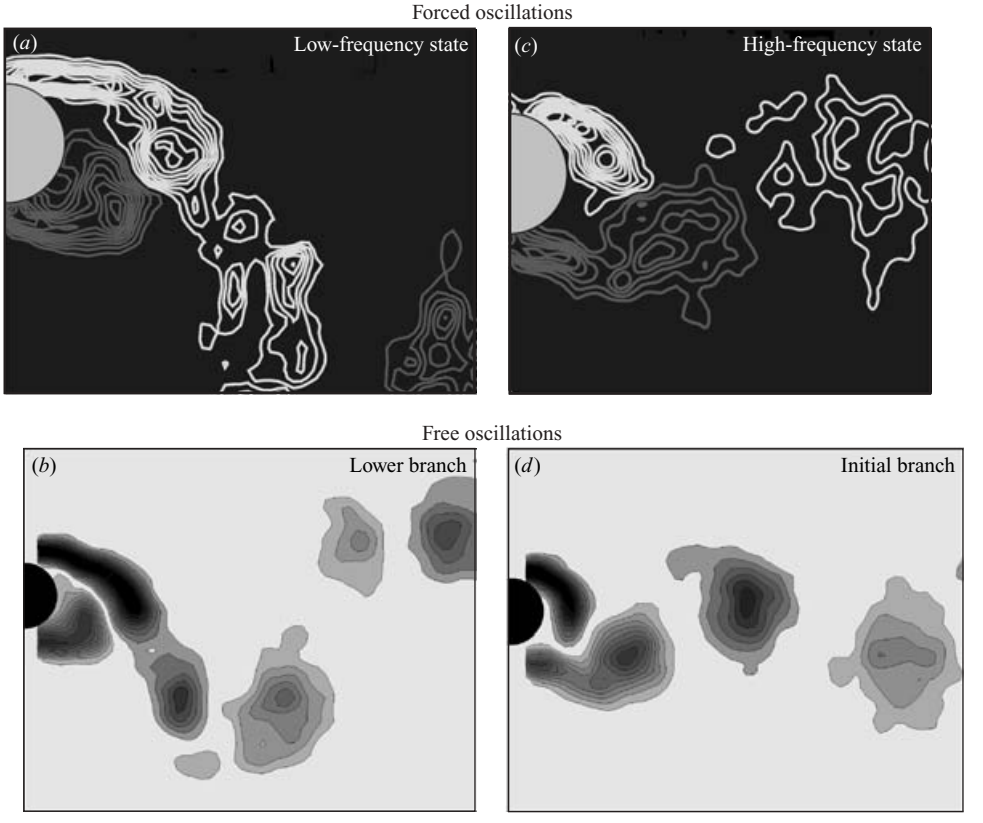

FIGURE 17. Phase-averaged vorticity fields at the top of the cylinder's oscillations for (*a*) forced oscillations, low-frequency state, $A/D = 0.6$, $f_e/f_o = 0.82$, $Re = 2300$; (*b*) free oscillations, lower branch, $A/D = 0.6$, $U^* = 6.40$, $Re = 3700$; (*c*) forced oscillations, high-frequency state, $A/D = 0.25$, $f_e/f_o = 1.15$, $Re = 4410$; (*d*) free oscillations, initial branch, $A/D = 0.33$, $U^* = 5.18$, $Re = 3000$. The fields for the freely oscillating cylinder are reproduced from Govardhan & Williamson (2000).

2P. The lower response branch occurs at higher reduced velocities which, as discussed previously, are equivalent to lower values of f_e/f_o. For the low-frequency and lower branch wakes in figure 17 the corresponding values of ϕ_{lift} and $\phi_{L\,vortex}$ are similar; however for the free and forced cases the lift phases lie either side of 180°. The phase of the vortex lift force for the low-frequency wake, shown in figure 17(*a*), is 184°, while for the lower branch, figure 17(*b*), $\phi_{L\,vortex}$ is just under 180°. Thus, the energy transfers for the forced and free cases are in opposite directions. Due to the vectorial relationship between the almost out-of-phase lift force and the apparent mass force, demonstrated in figure 8, the difference in the values of ϕ_{lift} for the low-frequency state and lower response branch is greater than the difference in $\phi_{L\,vortex}$.

The mode of vortex shedding for both the high-frequency and initial branch wakes in figures 17(*c*) and 17(*d*) are 2S and the structure of the wakes are very similar. The high-frequency state occurs at oscillation frequencies of $f_e/f_o > 1$ and equivalently the initial response branch occurs at $(U^*/f^*)St_o < 1$. There is a significant difference in the values of $\phi_{L\,vortex}$ for the high-frequency and initial branch wakes shown in figures 17(*c*) and 17(*d*). For the high-frequency state $\phi_{L\,vortex} = -78°$, whilst for the initial branch $\phi_{L\,vortex}$ is just greater than 0°. The large difference in $\phi_{L\,vortex}$ is consistent

with a shift in the phase of vortex shedding; however it is difficult to quantify the difference in phase from the vorticity fields of figures 17(*c*) and 17(*d*). The energy transfer for the initial branch is small and positive, while for the high-frequency state the energy transfer is negative and relatively large. Additionally, as the freely oscillating cylinder moves from the lower to the initial response branch there is a jump in the lift phase that is similar in magnitude and direction to the jump observed at the transition between the low- and high-frequency states. The jump in the vortex or total lift phase for the freely oscillating cylinder must always be less than 180°, as $0° < (\phi_{lift}$ or $\phi_{L\,vortex}) < 180°$. Therefore, using the plotting convention employed in this paper, the jump in the lift phase at the transition between different wake states/branches is generally greater for the case where the cylinder is forced to oscillate.

In summary, the low- and high-frequency wake states for the forced oscillations correspond respectively to the lower and initial response branches of the freely oscillating, elastically mounted cylinder. The structure of the near wake and the mode of vortex shedding for the forced and freely oscillating cylinders appear to be very similar. In both cases, the transition between two distinctly different wakes corresponds to an abrupt change in the forces on the cylinder. However, the fact that for the two cases shown in figure 17 the forced oscillations have negative energy transfer means that they do not predict the flow-induced motion. This indicates that the forced purely sinusoidal oscillations do not fully represent the almost sinusoidal motion of the freely oscillating cylinder.

9. Conclusions

In this work, we have described in considerable detail the wake states of a cylinder forced to oscillate transversely to a free stream. The nature of the interaction between the natural instability of the wake and the oscillation of the cylinder was studied using simultaneous measurements of the vortex structures in the near wake and the forces on the cylinder.

The manner in which the wake varies with the frequency of oscillation was examined for a range of A/D and Re. For the cases examined in our experiments, the wake spends the majority of its time in one of either of two stable wake states. Primarily, these wake states depend on the normalized frequency of oscillation, f_e/f_o, and thus we characterize these states as the low- and high-frequency wake states. The structure of the near wake and, in particular, the timing of vortex shedding, is distinctly different for the two wake states. These differences can be characterized in terms of a number of universal features, which were observed over the full range of A/D and Re studied. The phase of vortex shedding relative to the cylinder motion varies only slightly with A/D and Re and appears to depend primarily on the wake state. The phases of the vortex lift, $\phi_{L\,vortex}$, and drag, ϕ_{drag}, forces are directly related to the timing of large-scale changes in the vorticity field relative to the cylinder motion, and, as shown in figure 12, the low- and high-frequency wake states have characteristic values of $\phi_{L\,vortex}$ and ϕ_{drag}. The two wake states can also be characterized by the structure of the near wake and typically the mode of vortex shedding. The low-frequency wake state generates long attached shear layers, which, except for very low values of A/D, result in the 2P mode of vortex shedding. The high-frequency wake state has a much shorter wake length and vortices are shed in the 2S or Kármán mode.

As the wake makes the transition between the low- and high-frequency states there is a change in the phase of vortex shedding relative to the cylinder motion, and a corresponding jump in the phase of the vortex lift and drag forces. However, because

at transition there is also a change in the mode of vortex shedding, it is difficult to directly compare the change in timing of vortex shedding with the change in the values of $\phi_{lift\,vortex}$ and ϕ_{drag}. At transition there is also a jump in the values of C_L and $C_{L\,vortex}$; however, surprisingly, there are only relatively small changes in the values of C_D and $C_{D\,mean}$. While the jump in the phase of the vortex lift and drag at transition is relatively independent of A/D and Re, the jump in the magnitude of both the vortex and total lift forces depends on both variables.

For some values of A/D and Re, there is a self-excited transition between wake states at a constant frequency of oscillation. Therefore, for a small region of parameter space, both states can exist at different times. Usually, one of these states appears to be metastable; its existence depends on the startup conditions. During the self-excited transition, the vortex shedding mode and forces on the cylinder vary smoothly in the time domain between the low- and high-frequency wake states. This contrasts with the abrupt jump between the two stable states in the frequency domain.

The relative stability of the two wake states, and their susceptibility to transition, varies with f_e/f_o. As f_e/f_o changes a number of variables, including the natural frequency of the oscillating wake, respond in a nonlinear fashion and it is not possible to quantify the relationship between the stability of the wake states and f_e/f_o. However, there are a number of systematic changes that occur as f_e/f_o increases towards transition. For the low-frequency wake state, the length of the wake contracts as f_e/f_o increases, and there is greater disparity in the relative strength of the vortices that pair to produce the 2P pattern. As the wake approaches transition from either higher or lower f_e/f_o, the oscillation frequency f_e and the natural frequency of the oscillating wake f_{nos} converge, and at transition, f_e/f_{nos} jumps through unity. Despite these systematic changes, for a given wake state, the general characteristics of that state, in particular the phase of vortex shedding, remain relatively constant.

The total lift force on the oscillating cylinder can be decomposed into two components, as described in § 6.1: an apparent mass force F_{am} and a vortex force F_{vortex}. When the total lift force, $C_L(t)$, and the vortex lift force, $C_{L\ vortex}(t)$, are compared with the phase of vortex shedding for a range of flow parameters, it becomes evident that F_{vortex} is more appropriate than F_{total} in interpreting the force due to the vorticity field.

One of the major unsolved problems for this class of flows is whether the results of forced oscillation experiments can be used to predict the vortex-induced vibration of a structure that is free to oscillate. Whilst this investigation did not seek to answer this question a number of interesting issues have arisen. The relationship between a cylinder forced to oscillate with a pure sinusoidal motion and an elastically mounted cylinder is surprisingly complicated. However, there are striking similarities in the structure of the wake and the phase of the lift force for the forced and freely oscillating cylinders, and in both cases the wake undergoes a transition close to $f_e/f_o \approx 1$. The mode and timing of vortex shedding for the low-frequency state is very similar to that observed for the lower branch of the freely oscillating cylinder. Following transition to the high-frequency state, this state and the initial branch of the freely oscillating cylinder share the same general mode of shedding; however, the phase of the lift force is different. The difference in the phase of the lift force equates to a change in the direction of energy transfer from positive for the elastically mounted cylinder, to negative for the forced oscillations, thus emphasizing one of the fundamental differences between the forced and freely oscillating cases. Interestingly, the results of these, and previous, investigations show that the forced oscillations can result in negative energy transfer for purely sinusoidal motion at frequencies and

amplitudes at which free vibrations are known to occur. This suggests that small differences in the motion of the cylinder can result in significant changes in the energy transfer. Therefore, despite encouraging similarities in the wake states of the forced and free oscillations, further work is required to determine how the forced case can be used to predict the vortex-induced motion.

Primary support for this research program was provided by the Office of Naval Research Grant N00014-94-1-0815, P0006, monitored by Dr Thomas Swean, and by the Australian Research Council through the ARC Large Grant A89702238. In addition, supplemental support was provided by NSF Grant CTS-9803734. J. C. acknowledges support through an Australian Postgraduate Award. The authors gratefully acknowledge this financial support.

REFERENCES

Bearman, P. W. 1984 Vortex shedding from oscillating bluff bodies. *Annu. Rev. Fluid Mech.* **16**, 195–222.

Bishop, R. E. D. & Hassan, A. Y. 1963 The lift and drag forces on a circular cylinder in a flowing fluid. *Proc. R. Soc. Lond.* A **277**, 32–50.

Blackburn, H. M. & Henderson, R. D. 1999 A study of two-dimensional flow past an oscillating cylinder. *J. Fluid Mech.* **385**, 255–286.

Blackburn, H. M. & Melbourne, W. H. 1997 Sectional lift forces for an oscillating circular cylinder in smooth and turbulent flows. *J. Fluids Struct.* **11**, 413–431.

Blevins, R. D. 1990 *Flow-induced Vibration.* Van Nostrand Reinhold.

Brika, D. & Laneville, A. 1993 Vortex-induced vibrations of a long flexible circular cylinder. *J. Fluid Mech.* **250**, 481–508.

Carberry, J. 2002 Wake states of a submerged oscillating cylinder and of a cylinder beneath a free-surface. PhD thesis, Monash University, Melbourne, Australia.

Carberry, J., Sheridan, J. & Rockwell, D. 2001 Forces and wake modes of an oscillating cylinder. *J. Fluids Struct.* **15**, 523–532.

Deniz, S. & Staubli, T. 1997 Oscillating rectangular and octagonal profiles: interaction of leading- and trailing-edge vortex formation. *J. Fluids Struct.* **11**, 3–31.

Deniz, S. & Staubli, T. 1998 Oscillating rectangular and octagonal profiles: modelling of fluid forces. *J. Fluids Struct.* **12**, 859–882.

Feng, C. C. 1968 The measurements of vortex-induced effects in flow past a stationary and oscillating circular and D-section cylinders. Master's thesis, University of British Columbia, Vancouver, B.C., Canada.

Gopalkrishnan, R. 1993 Vortex induced forces on oscillating bluff cylinders. MIT Doctoral Dissertation.

Govardhan, R. & Williamson, C. H. K. 2000 Modes of vortex formation and frequency response of a freely vibrating cylinder. *J. Fluid Mech.* **420**, 85–130.

Gu, W., Chyu, C. & Rockwell, D. 1994 Timing of vortex formation from an oscillating cylinder. *Phys. Fluids* **6**, 3677–3682.

Huerre, P. & Monkewitz, P. A. 1990 Local and global instabilities in spatially developing flows. *Annu. Rev. Fluid Mech.* **22**, 473–537.

Karniadakis, G. E. M. & Triantafyllou, G. S. 1989 Frequency selection and asymptotic states in laminar wakes. *J. Fluid Mech.* **199**, 441–469.

Khalak, A. & Williamson, C. H. K. 1999 Motions, forces and mode transitions in vortex-induced vibrations at low mass-damping. *J. Fluids Struct.* **13**, 813–851.

Leonard, A. & Roshko, A. 2001 Aspects of flow-induced vibration. *J. Fluids Struct.* **15**, 415–425.

Lotfy, A. & Rockwell, D. 1993 The near-wake of an oscillating trailing edge: mechanisms of periodic and aperiodic response. *J. Fluid Mech.* **251**, 173–201.

Mercier, J. A. 1973 Large amplitude oscillations of a circular cylinder in a low-speed stream. Stevens Institute of Technology, PhD.

Naudascher, E. & Rockwell, D. 1994 *Flow-induced Vibrations: An Engineering Guide*. A. A. Balkema.

Noca, F. 1997 On the evaluation of time-dependent fluid-dynamic forces on bluff bodies. PhD Thesis, California Institute of Technology.

Ongoren, A. & Rockwell, D. 1988 Flow structure from an oscillating cylinder Part 1. mechanisms of phase shift and recovery in the near wake. *J. Fluid. Mech.* **191**, 197–223.

Pantazopoulos, M. S. 1994 Vortex-induced vibration parameters: critical review. *OMAE, Offshore Technology*. ASME, vol. 1, pp. 199–255.

Rockwell, D., Magness, C., Towfighi, J., Akin, O. & Corcoran, T. 1993 High image-density particle image velocimetry using laser scanning techniques. *Exp. Fluids* **14**, 181–192.

Sarpkaya, T. 1978 Fluid forces on oscillating cylinders. *J. Waterway Port Coastal Ocean Div. ASCE* **104**, 275–290.

Sarpkaya, T. 1995 Hydrodynamic damping, flow-induced oscillations, and biharmonic response. *ASME J. Offshore Mech. Artic Engng* **177**, 232–238.

Stansby, P. K. 1976 The locking-on of vortex shedding due to the cross-stream vibration of circular cylinders in uniform and shear flows. *J. Fluid Mech.* **74**, 641–665.

Staubli, T. 1983*a* Calculation of the vibration of an elastically mounted cylinder using experimental data from forced oscillation. *Trans. ASME: J. Fluids Engng* **105**, 225–229.

Staubli, T. 1983*b* Untersuchung der oszillierenden Krafte am querangestromten, schwingenden Kreiszylinder. Dissertation ETH 7322.

Staubli, T. & Rockwell, D. 1989 Pressure fluctuations on an oscillating trailing edge. *J. Fluid Mech.* **203**, 307–346.

Szechenyi, E. & Loiseau, H. 1975 Portances instantionnaires surun cylinder vibrant dans un ecoulement supercritique. (Fluctuating lift on a cylinder vibrating in supercritical flow). *La Recherche Aerospatiale* **1**, 45–57.

Williamson, C. H. K. & Roshko, A. 1988 Vortex formation in the wake of an oscillating cylinder. *J. Fluids Struct.* **2**, 355–381.

Wu, J. C. 1981 Theory for aerodynamic force and moment in viscous flows. *AIAA J.* **19**, 432–441.